

General Disclaimer

One or more of the Following Statements may affect this Document

- This document has been reproduced from the best copy furnished by the organizational source. It is being released in the interest of making available as much information as possible.
- This document may contain data, which exceeds the sheet parameters. It was furnished in this condition by the organizational source and is the best copy available.
- This document may contain tone-on-tone or color graphs, charts and/or pictures, which have been reproduced in black and white.
- This document is paginated as submitted by the original source.
- Portions of this document are not fully legible due to the historical nature of some of the material. However, it is the best reproduction available from the original submission.

CR 167 833
C.1



Battelle

Columbus Laboratories

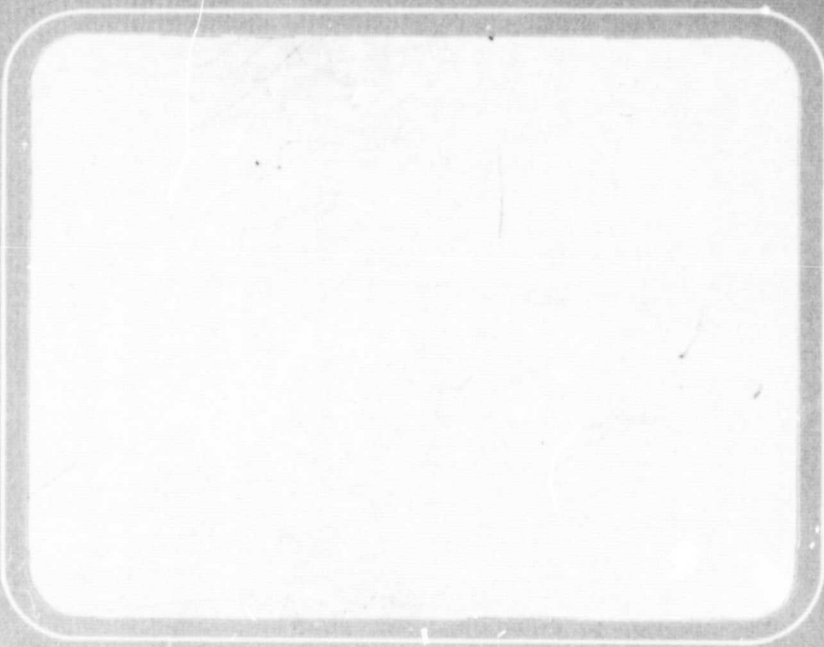
(NASA-CR-167833) AN ASSESSMENT OF POTENTIAL
DETECTORS TO MONITOR THE MAN-MADE ORBITAL
DEBRIS ENVIRONMENT Final Report (Battelle
Columbus Labs., Ohio.) 107 p HC A06/MF A01

N83-20974

Unclas
03235

CSCL 22A G3/12

Report



ORIGINAL PAGE IS
OF POOR QUALITY

FINAL REPORT

on

AN ASSESSMENT OF POTENTIAL DETECTORS
TO MONITOR THE MAN-MADE
ORBITAL DEBRIS ENVIRONMENT

to

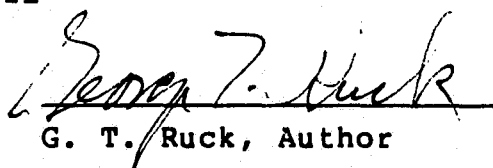
NATIONAL AERONAUTICS AND
SPACE ADMINISTRATION

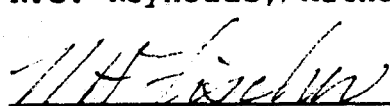
Johnson Space Center

February 28, 1983

Contract NAS9-16721


R.C. Reynolds, Author


G. T. Ruck, Author


Approved by: N.H. Fischer, Manager
Space Systems Section

BATTELLE
Columbus Laboratories
505 King Avenue
Columbus, Ohio 43201

TABLE OF CONTENTS

ORIGINAL PAGE IS
OF POOR QUALITY

	<u>Page</u>
1.0 INTRODUCTION	1-1
1.1 Study Objectives.	1-3
1.2 Problem Background.	1-3
1.3 Design Response to Projected Debris Hazard.	1-9
1.4 Roles and Options for Detection Systems	1-12
2.0 CURRENT AND PROJECTED HAZARD LEVELS.	2-1
2.1 Current Hazard Levels	2-1
2.2 Projected Hazard Levels	2-11
2.3 Definition of Reference Populations	2-27
2.4 Detection Ranges.	2-29
3.0 DETECTOR SYSTEMS--LARGE PARTICLES.	3-1
3.1 Ground-Based Systems.	3-1
3.2 Space Qualified Systems	3-5
3.3 Evaluation of Options	3-11
4.0 MICROPARTICLE DETECTOR SYSTEMS	4-1
4.1 Impact Sensors.	4-1
5.0 EVALUATION OF THE "PIGGY-BACK" OPTION.	5-1
5.1 Sharing the Ride on Free-Flyers	5-1
5.2 Working From the Shuttle in a Non-Deploy Mode	5-13
5.3 Making Use of Available Data.	5-16
6.0 CONCLUSIONS.	6-1
7.0 REFERENCES	7-1
APPENDIX A.	A-1

1.0 INTRODUCTION

Debris in low Earth orbit (LEO) has an orbital speed of about 25,000 ft/sec (7 km/sec). Because of the diverse inclinations and plane orientations of the orbits of material in this region, relative velocities between colliding objects will be, on the average, about orbital velocity. This means that particles as small as milligram size (on the order of a millimeter in diameter) could disable an operating spacecraft on impact, while objects of microgram size might degrade the resolution in spacecraft optics and impair the efficiency of its solar panels. Observations using NORAD radar have shown that man-made debris exceeds the natural environment for large (>4 cm) objects. For short times (a few days to a few weeks) after solid rocket motor (SRM) firings in LEO, man-made debris in the microparticle size range also appears to exceed the meteoroid environment. The properties of the debris population between these size regimes is currently unknown as there has been no detector system able to perform the required observations. However, obtaining data on the unobserved debris is important for two reasons: (1) it is needed to fully understand the threat to current space systems, and (2) debris in this size range may play an important role in the population evolution so that knowledge of its current state would be an essential ingredient in assessing the threat to future space systems. The primary objective of this study is to assess the alternatives for obtaining data on this currently unobserved segment of the population.

In this study the distinction between debris which poses a lethal threat to unprotected spacecraft ("large" debris) versus a threat to degrade its operational capability (microparticle debris) is based on size, with 1 mm being the minimum size for large debris. The distinction based solely on size undoubtedly oversimplifies the problem of spacecraft vulnerability to debris, but until adequate vulnerability analysis

becomes available for projectiles in the mass range of 100 μ grams to 100 grams this simplification appears defensible.

The accommodation of future space operations to the presence of debris in the operating environment will require a prediction of the threat which the debris will pose. Based on the nature of the threat, specifically the mass spectrum and kinematic properties of the debris population, design and operational alternatives will have to be evaluated. The projection of future debris states will require data on the current state (the zero-time state) as well as a suitable model for future source contributions. At the present time there is insufficient data for an adequate zero-time model for the larger objects. Some data on the microparticle debris may indicate a satisfactory zero-time model for that debris can be produced.

This introductory section is used to present the study objectives, a brief review of the debris problem (threat characterization) and general considerations on design responses, and a discussion of the role detectors play in the overall problem analysis. A more detailed discussion of the current and future hazard levels arising from large debris is presented in Section 2: based on this discussion, population standards are established and required detector scan volumes are related to the associated flux levels. Microparticle debris is also discussed in Section 2. Sections 3 and 4 present discussion of detector systems for both large particles and microparticles based on the available technology. For large particle detectors, both ground-based and orbital systems are surveyed. The possibility of "piggy-backing" as a cost-effective alternative in acquiring debris data is presented in Section 5; the conventional concept of piggy-backing to make use of power, telemetry, and orientation control is one aspect examined, others being processing of acquired data and making use of exposed surfaces on retrievable spacecraft. The summary and conclusions are presented in Section 6.

1.1 STUDY OBJECTIVES

The primary objective of this study is to examine the alternatives for obtaining adequate information on the man-made debris population in LEO. This entails an assessment of current technology capabilities, likely near-term technology developments, projected debris states, and projected space traffic. The emphasis has been on the large, and therefore potentially lethal, debris but parallel consideration is provided for the micro-particle environment. A secondary objective of this study is to evaluate the impact of debris on future spacecraft design practices.

1.2 PROBLEM BACKGROUND

Two types of observations have been conducted to detect debris in LEO. NORAD radar has been used to detect and track the larger man-made debris objects to produce catalogues of the orbital elements of the debris; these data have been used to deduce time-averaged spatial densities and, by including radar cross-section data, indirect evidence on the size and mass distribution of the debris [Kessler and Cour-Palais, 1978]. Impact sensors have also been flown in LEO to monitor the microparticle debris population; these data lead to debris fluxes and, using momentum or energy arguments, information on the mass distribution.

These observable quantities may be related directly to collision probabilities and to expected time between collisions, two quantities which characterize the hazard level. The relationship between the debris flux, f , and the debris density, n , is

$$f = nvR$$

(1.2-1)

where v_R is the speed of the detector relative to the debris.
The probability that a vehicle experience at least one collision,
 P_C , is

$$P_C = 1 - e^{-f\sigma T} \quad (1.2-2)$$

where σ = collision cross-section
 T = time spent in the environment

The expected time between collisions, τ , is defined to
be

$$\tau \equiv 1/f\sigma \quad (1.2-3)$$

which is the time for which the collision probability is $(1-1/e)$.
If the expected mission time for a given space system exceeds τ ,
collisions with debris might be expected to occur. Figure 1.2-1
presents τ for a set of spatial densities, assuming a relative
velocity of 7 km/sec. For current tracked debris in LEO, debris
densities of 10^{-8} to 10^{-11} are encountered.

The concern for orbital debris is the hazard it pre-
sents to space systems. To protect against this threat, there is
a need to know what sized particle must be protected against.
Therefore, for hazard analysis the most useful plot is the cumu-
lative flux vs mass, as shown in Figure 1.2-2, where cumulative
flux, f_M , is defined to be the flux of particles of mass $> M$.
The probability of colliding with an object at least as large as
 M , P_C^M , is given by

$$P_C^M = 1 - e^{-f_M\sigma T} \quad (1.2-4)$$

If a hit on a spacecraft by an object of mass $> M$ is
taken to be a kill of that spacecraft, the survival probability,
 S_C^M , is

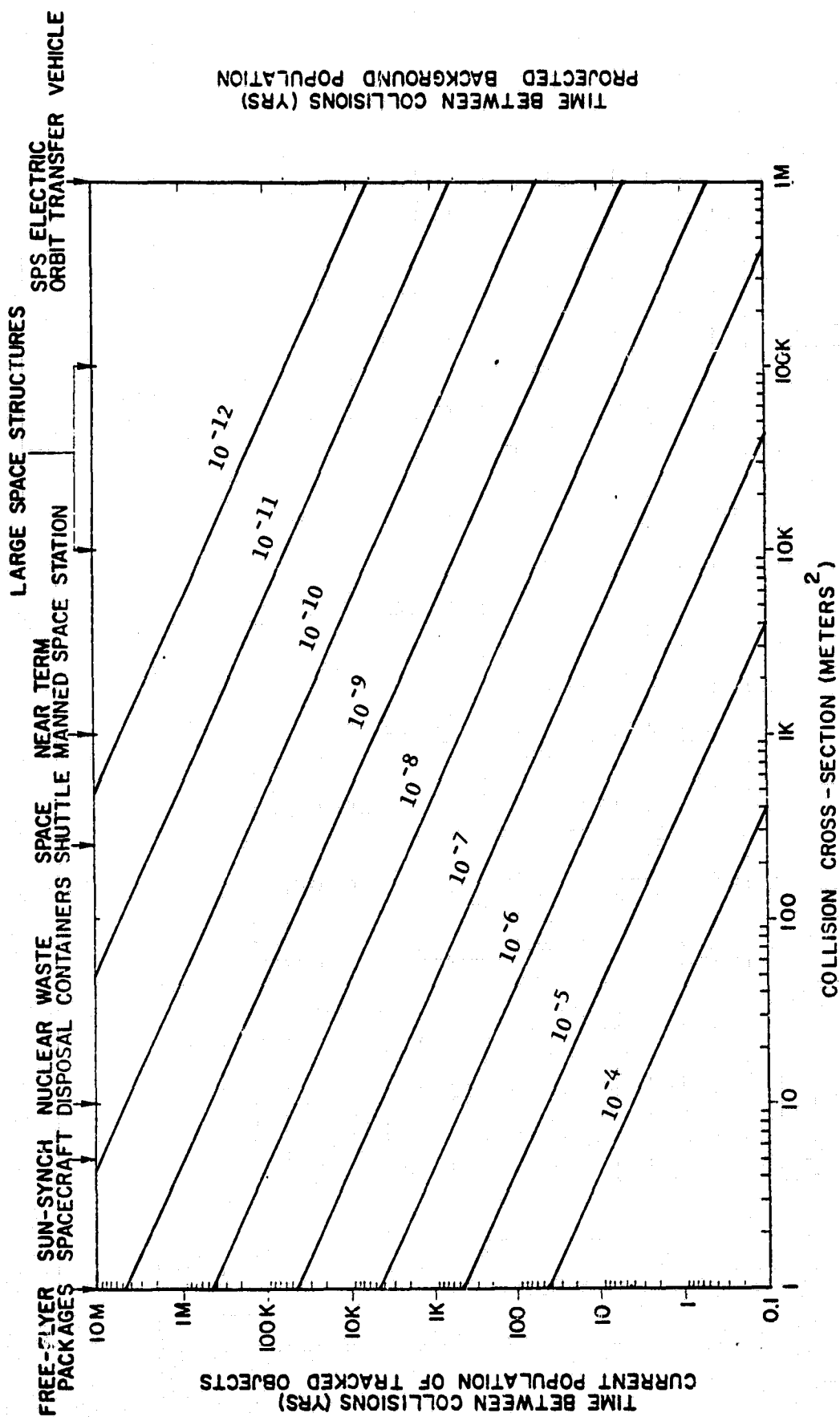


FIGURE 1.2-1. EXPECTED TIME BETWEEN COLLISIONS AS A FUNCTION OF COLLISION CROSS-SECTION FOR A RANGE OF DEBRIS DENSITIES

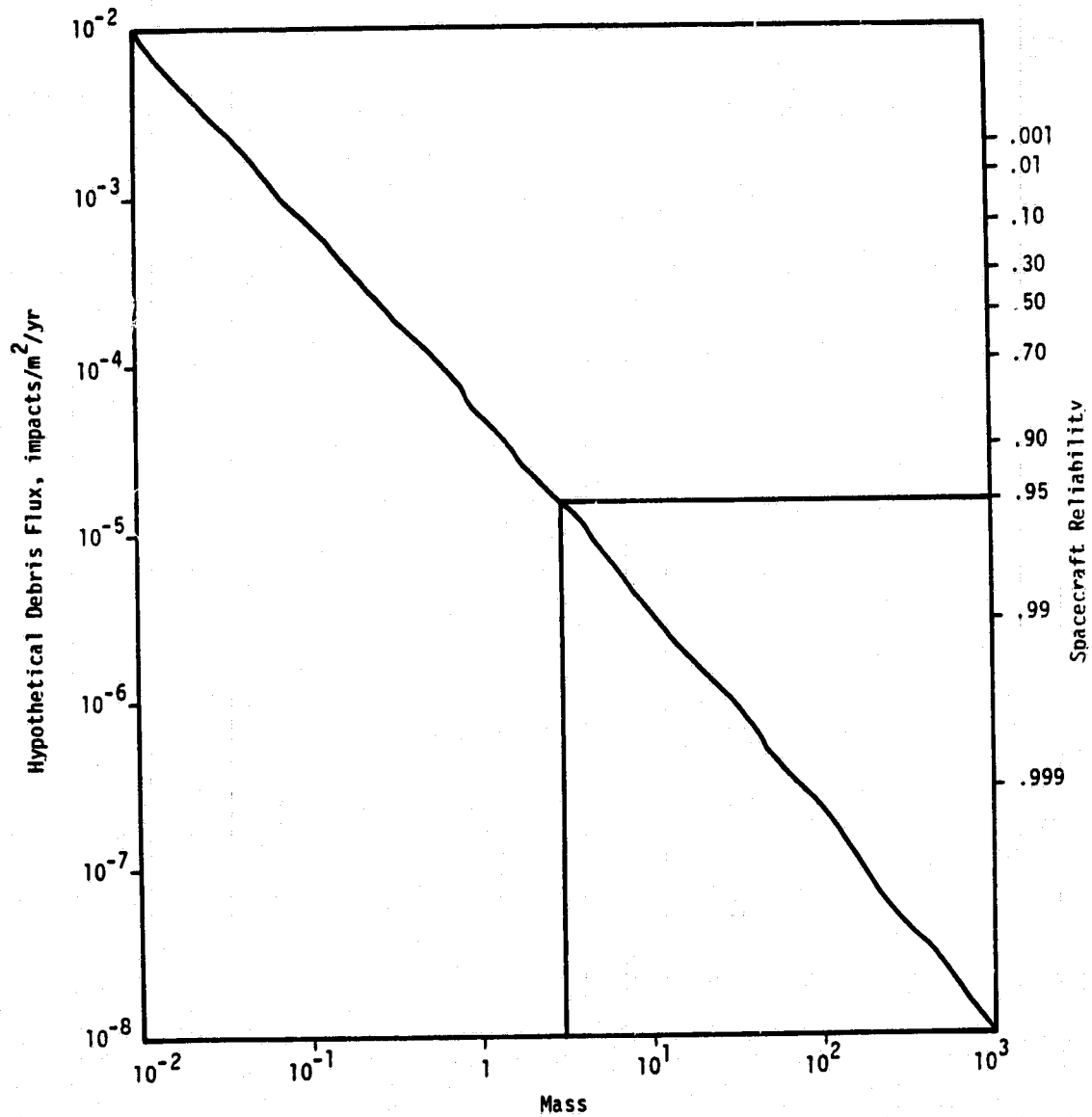


FIGURE 1.2-2. CUMULATIVE DEBRIS FLUX & SPACECRAFT SURVIVAL PROBABILITY FOR A HYPOTHETICAL DEBRIS POPULATION

$$S_C^M = 1 - P_C^M = e^{-f_M \sigma T} \quad (1.2-5)$$

Figure 1.2-2 can therefore also represent a scale of survival probability in the presence of a debris hazard. The translation is given in Table 1.2-1.

TABLE 1.2-1. RELATION BETWEEN COLLISION PROBABILITY, SURVIVAL PROBABILITY, AND DEBRIS HAZARD PARAMETERS

P_C^M	S_C^M	$f_M \sigma T$
0.001	0.999	0.001
0.01	0.99	0.01
0.05	0.95	0.05
0.10	0.90	0.11
0.30	0.70	0.36
0.50	0.50	0.69
0.70	0.30	1.20
0.90	0.10	2.30
0.95	0.05	3.00
0.99	0.01	4.61
0.999	0.001	6.91

This translation, for some value of σ , given by the type of spacecraft, and T , given by the mission time, is provided on the right-hand axis of Figure 1.2-2. In the case shown, for 95 percent survivability, debris as large as size 3 must be protected against.

Uncertainties in the properties of the debris population replace the line in Figure 1.2-2 with a band, as shown in Figure 1.2-3. These uncertainties arise from limitations on the observational data - restrictions on the sampling volume, contributions from non-random states, and limits on the size of the observable objects - as well as uncertainties introduced by future source contributions. In the example shown in Figure 1.2-3 the minimum population would require protecting only to

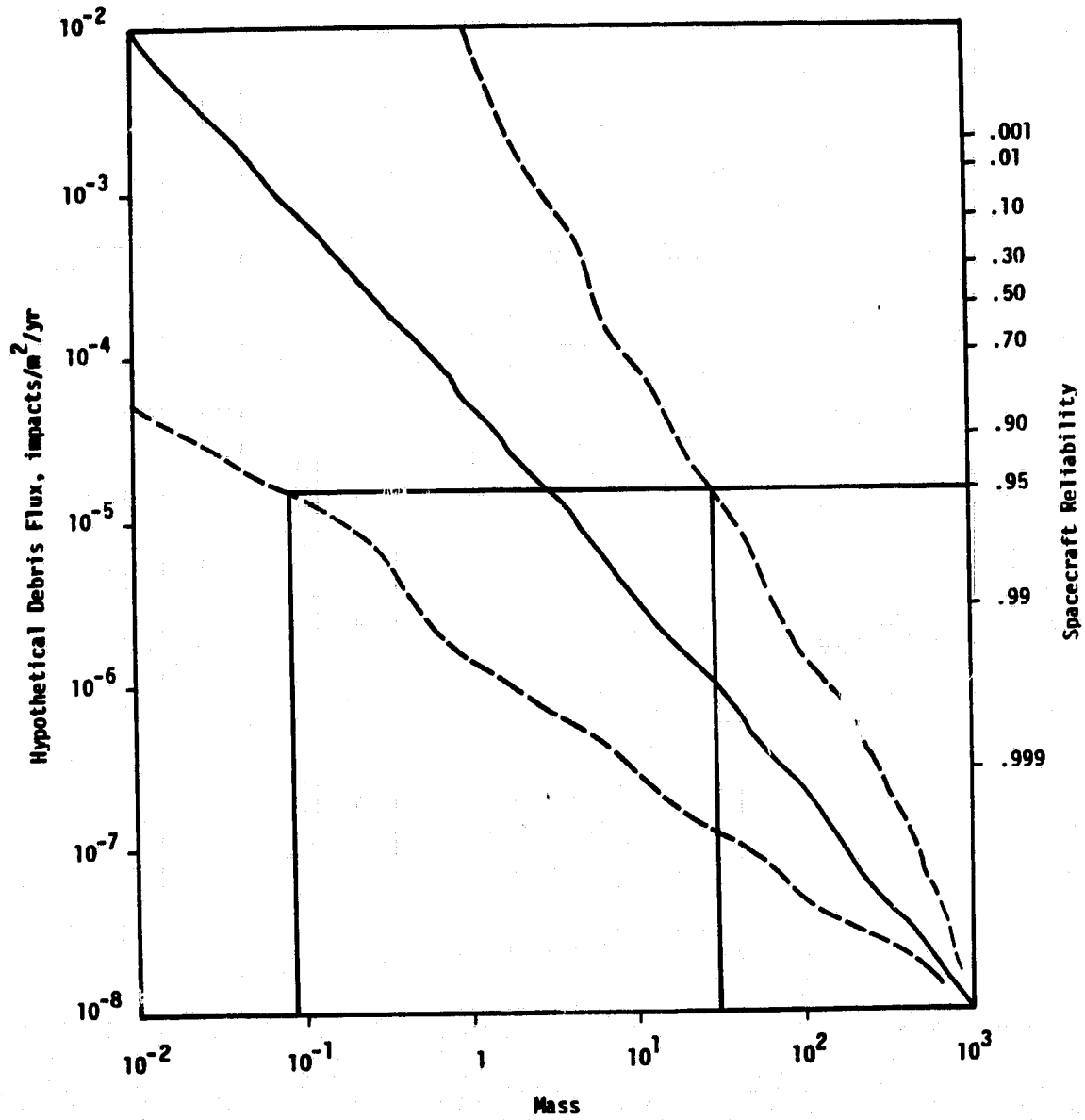


FIGURE 1.2-3. CUMULATIVE DEBRIS FLUX & SPACECRAFT SURVIVAL PROBABILITY FOR A HYPOTHETICAL DEBRIS POPULATION

mass 0.09 to ensure 95 percent survival probability, while the maximum population would require protecting to mass 30.0. In those actual cases where the lower mass value was considerably smaller than the larger, the impact of uncertainties in the debris population on spacecraft design and program cost would be significant.

Although the dominant uncertainty contributors will be different for short-term and long-term projections, a basic problem in debris work is to determine what the uncertainty ranges are and to provide recommendations to bound those uncertainties which can be estimated. This examination of detector options takes such a step.

1.3 DESIGN RESPONSE TO DEBRIS HAZARD

The problems associated with designing spacecraft and planning space programs in an era of hazard produced by man-made debris may require new approaches to spacecraft design. Although a similar type of problem was encountered because of the meteoroid threat, it was found that assurance of reliability in the presence of this threat was obtainable with spacecraft shielding. A significant threat level for man-made debris may arise from much larger particle mass and so much more complex solutions may be required.

In the classic approach to neutralizing the threat to a system, design practices in future eras will be the outcome of a three-step analysis procedure:

- (1) threat analysis
- (2) vulnerability analysis
- (3) survivability analysis.

The characterization of the threat has been discussed in the previous section and in a very schematic way can be described as in Table 1.3-1.

TABLE 1.3-1. NATURE OF THE DEBRIS THREAT AND POSSIBLE SOURCES FOR DEBRIS IN VARIOUS SIZE REGIMES

Debris Size (Mass)	Nature of Threat	Potential Sources
submillimeter (microgram)	degrade optics, solar panels	SRM exhaust, collisions, high-intensity explosions
millimeter (milligram)	penetrate unshielded spacecraft	collisions, explosions
centimeter (gram)	penetrate shielded spacecraft	collisions, explosions, normal operations
decimeter (kilogram)	fragment spacecraft	collisions, explosions, normal operations, s/c breakup

Because the meteoroid mass of concern in spacecraft design has been in the milligram regime, spacecraft shielding has provided acceptable protection. However, in an era with significant amounts of man-made debris, more elaborate alternatives will need to be assessed. Vulnerability analysis methodologies have been used successfully for aircraft, and much of the analysis can be carried over to the spacecraft arena. An example of such a methodology is presented in Figure 1.3-1, with an indication of those parts of the methodology which could be carried over to a spacecraft analysis.

Another aspect of the vulnerability analysis for spacecraft will be the operations alternatives, which include orbit selection, spacecraft (or subsystem) orientation, and maneuvering capability.

Survivability analysis will require an establishment of trade alternatives which can be evaluated and used as trade-off variables in the vulnerability analysis. Alternatives to be tested in a survivability analysis fall into three classifications, and a typical set of trade alternatives would be:

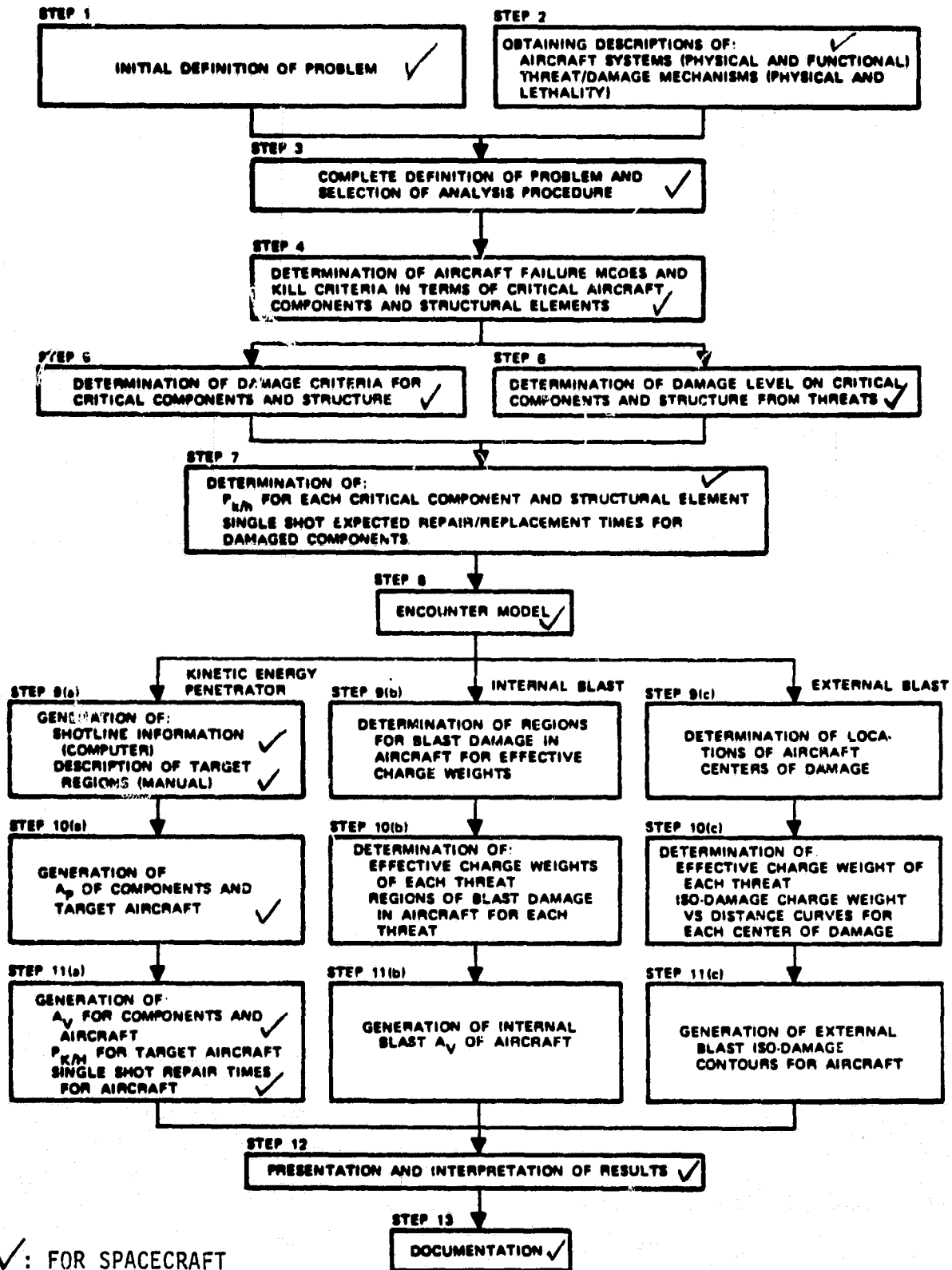


FIGURE 1.3-1. FLOW OF TYPICAL AIRCRAFT VULNERABILITY ANALYSIS

- (1) **Structural and design layout alternatives**
 - (a) spacecraft shielding
 - (b) component shielding
 - (c) component location
 - (d) subsystem redundancy
 - (e) damage localization
 - (f) "gentle" mission capability degradation
- (2) **Operational alternatives**
 - (a) detection and avoidance
 - (b) orbital maneuver capability
 - (c) mission profile/orbit selection
 - (d) active orientation control
- (3) **Programmatic alternatives**
 - (a) number of spacecraft
 - (b) separation of capability
 - (c) spacecraft lifetime.

Until future debris states can be produced with a satisfactory levels of confidence, the evaluation of alternatives cannot be carried out. For example, if reliability required protection only from microparticle debris, shielding of the spacecraft would probably be the effective solution. On the other hand, a requirement to protect from centimeter-sized objects would involve a much more complex analysis.

1.4 Roles and Options For Detection Systems

Debris detectors can serve 2 purposes - to monitor the debris population, i.e., provide information on the general properties of the debris population, or to provide data for specific localized response to a debris threat, as in detection and avoidance of population members. The concern in this work is the monitoring role.

For the large debris the options for placement of monitoring detectors are ground-based and orbital. Ground-based

systems have the advantage of essentially unlimited power availability, easy access for repair and enhancement, greater ease of modification, and greater ease of data storage. The disadvantage is remoteness from the scanned volume, which limits the minimum sized object which can be detected. Radar and passive optical systems are the most promising ground-based options. Orbiting debris detectors have the single advantage of being able to detect smaller particles but over reduced ranges. Radar and passive optical and IR systems are promising orbital systems. Orbiting radar would appear capable of detecting 1 mm particles to a distance of 10 km; passive IR, as indicated by the Infrared Astronomical Satellite (IRAS) detector sensitivities, could have 70 km limit at 1 mm a 7000 km range at 1 cm. Radar data can provide range and relative velocity information directly to establish the orbital properties and size of the debris. A passive system can only provide angular velocity and photon flux information; assumptions on the optical absorptivity and IR emissivity and observations in multiple frequency bands to establish temperature could be used with the angular velocity to establish statistical arguments on debris size. Establishing orbital elements from these observations does not appear feasible.

Orbiting systems are the only means for detecting microparticle debris, using impact sensors. Historically, pressurized cells and passive optical systems have been used in this work. However, with the availability of retrievable carriers, large, very simple impact recorders might prove useful.

2.0 CURRENT AND PROJECTED HAZARD LEVELS

2.1 CURRENT HAZARD LEVELS

2.1.1 Large Objects

A continued monitoring of large objects on orbit is conducted by NORAD, with data on the orbital elements of unclassified spacecraft appearing in reports such as the NASA Satellite Situation Report. The number of objects in this report has grown from about 4300 in 1976 to about 4900 in 1982. A reduction of this population to spatial densities is presented in Figure 2.1-1 for the October, 1976, report. It is in good agreement with similar figures presented by Kessler and Cour-Palais [1978] and Chobotov [1981].

This population presents no major hazard to existing space systems, as shown in Figure 2.1-2, although, as can also be seen in Figure 2.1-2, even this population begins to present a threat to some of the large space systems being considered for future space operations.

Several sources of observational limitation make this sample incomplete with respect to the total population of large debris and point to the need for an enhanced observational capability. First, the limiting detection size of the radar varies with altitude, as shown in Figure 2.1-3 [Kessler, 1982b], so that the sample is not uniform. Correction factors to account for this effect have been proposed by Kessler, based on an extrapolation of observed objects at lower altitude, and is presented in Figure 2.1-4. With these correction factors, the number of objects in LEO of size greater than 4 cm increases by a factor of 5, and the hazard at various altitudes increases as shown in Figure 2.1-5 [Kessler, 1981].

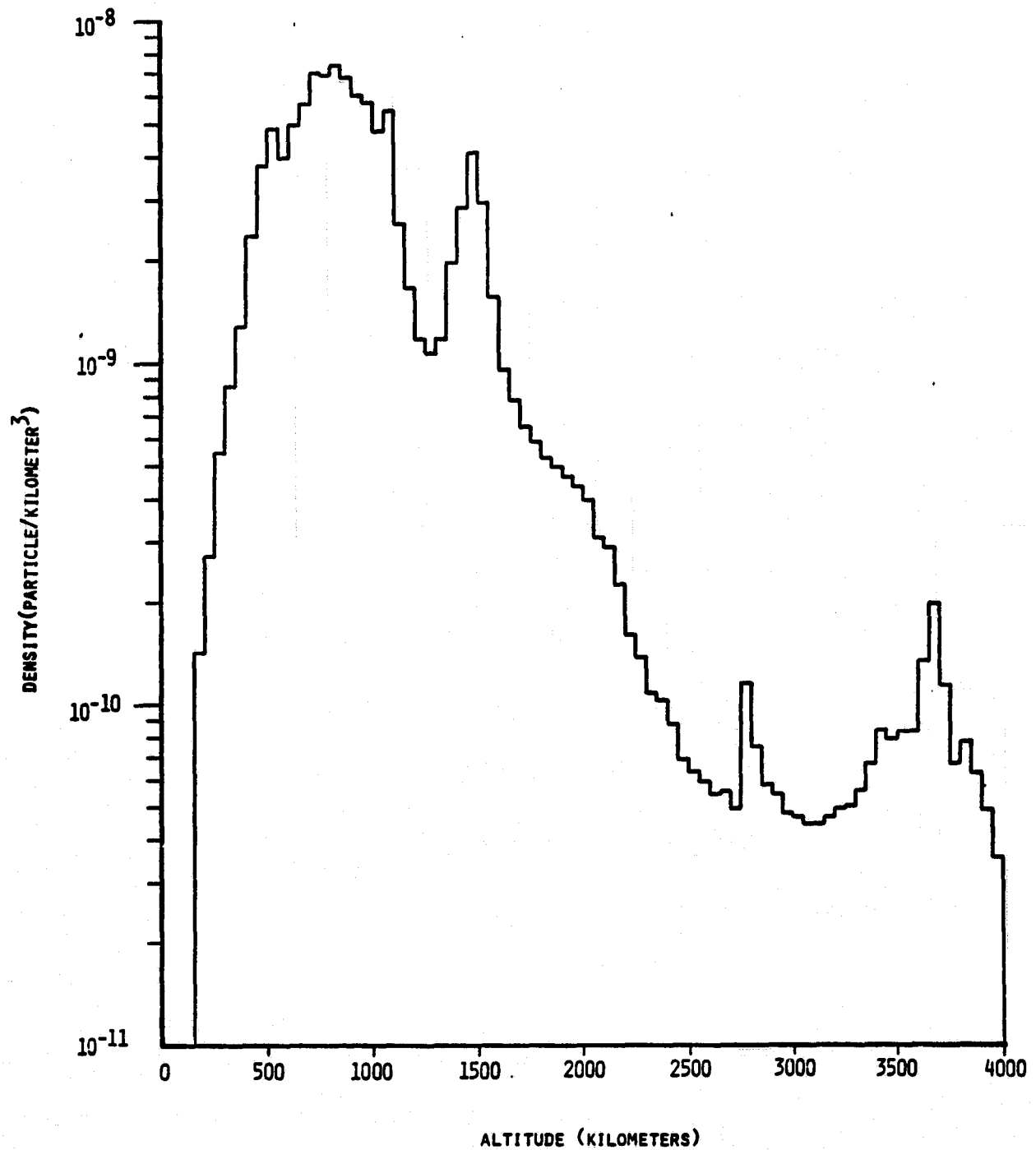


FIGURE 2.1-1. DENSITY OF TRACKED DEBRIS AS A FUNCTION OF ALTITUDE (OCTOBER, 1976, SATELLITE SITUATION REPORT, THE "ZERO TIME" POPULATION)

ORIGINAL PAGE IS
OF POOR QUALITY

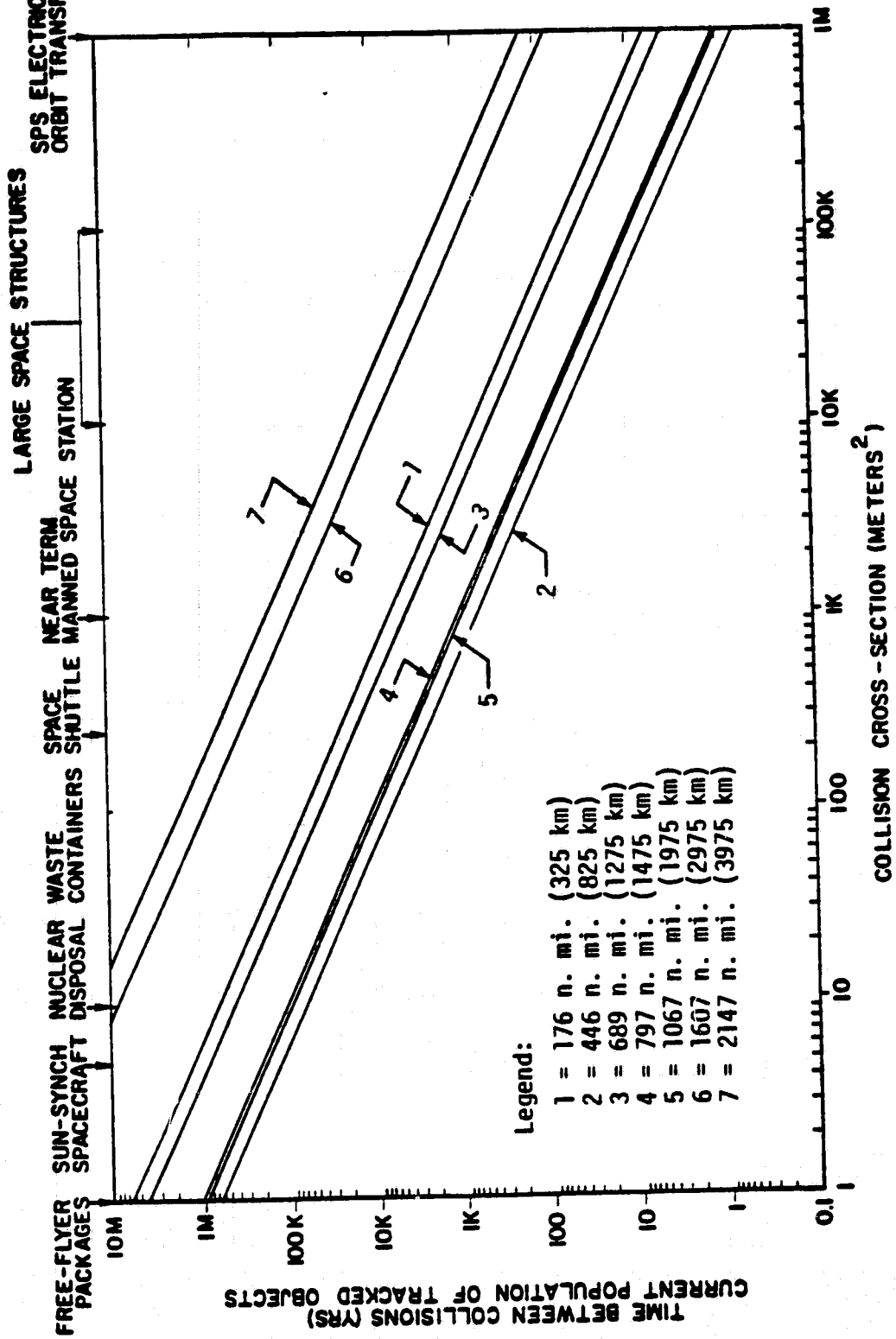


FIGURE 2.1-2. EXPECTED TIME BETWEEN COLLISIONS AS A FUNCTION OF COLLISION CROSS-SECTION FOR THE ZERO-TIME POPULATION OF TRACKED DEBRIS

ORIGINAL PAGE IS
OF POOR QUALITY

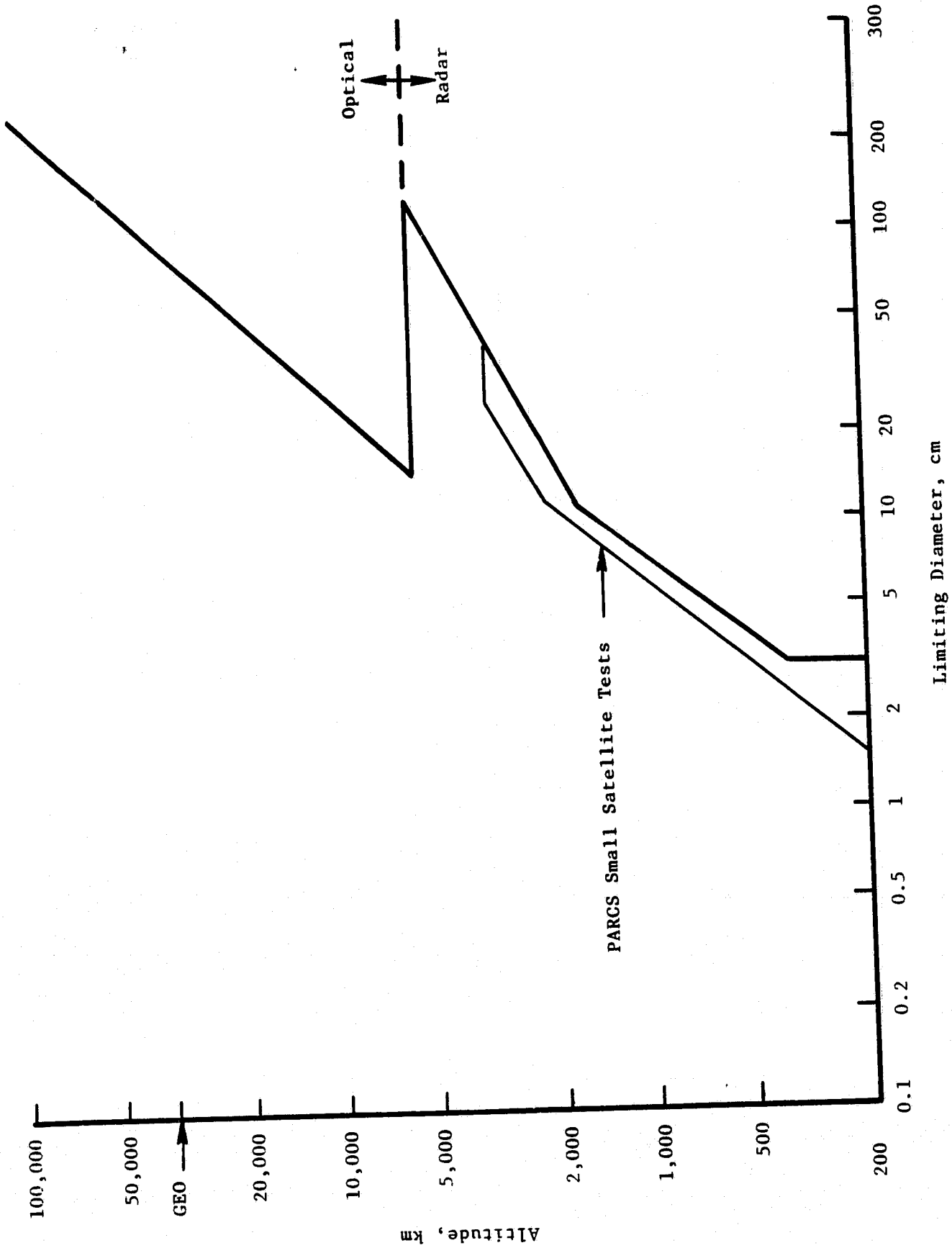


FIGURE 2.1-3. LIMITING DETECTION SIZE FOR NORAD DETECTOR SYSTEMS

ORIGINAL PAGE IS
OF POOR QUALITY

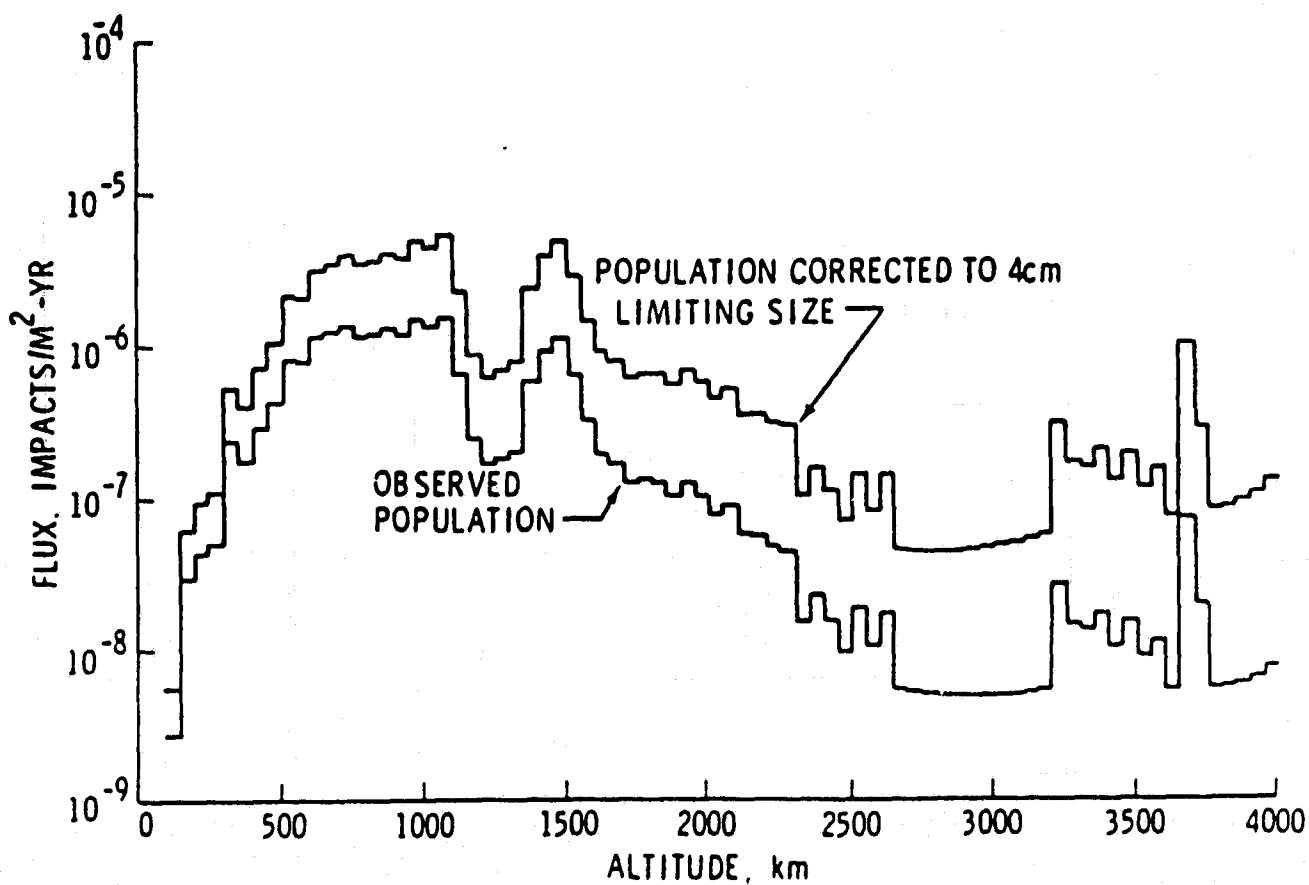


FIGURE 2.1-4. MAN-MADE DEBRIS FLUX CORRECTED TO 4-CM
LIMITING SIZE [KESSLER, 1981]

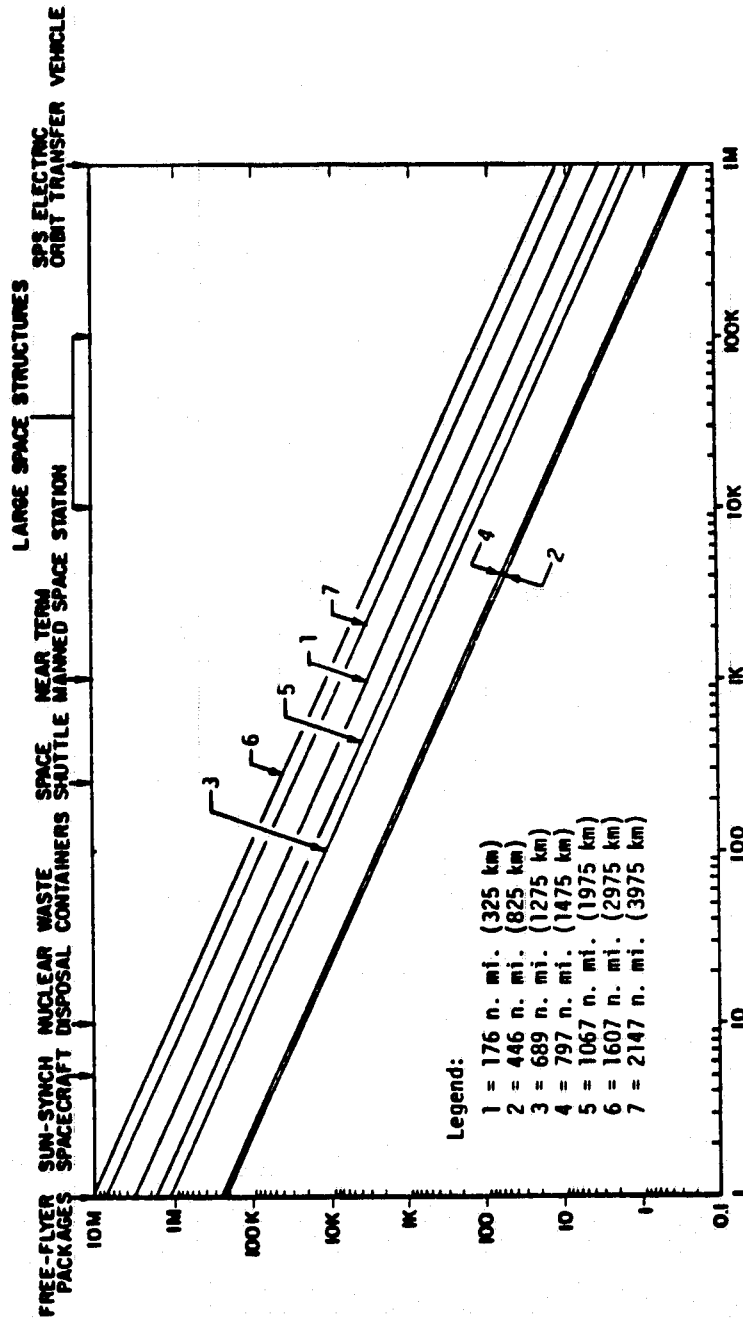


FIGURE 2.1-5. EXPECTED TIME BETWEEN COLLISIONS AS A FUNCTION OF COLLISION CROSS-SECTION FOR THE ZERO-TIME POPULATION CORRECTED TO SIZE 4 CM TO ACCOUNT FOR UNOBSERVED OBJECTS

A second source of incompleteness is introduced because NORAD instruments have only a subsidiary assignment to gather data on orbital debris so that the radar will only acquire and process data as can be accommodated by its primary detection and tracking tasks. Useful data may be discarded because insufficient resources exist to process it. Also, the radar have not been "tuned" to acquire data on small objects. Two tests of the NORAD PARCS radars have been conducted in which the radar were tuned and used in a dedicated debris detection mode. The result of these tests was that about 7 percent of the objects tracked did not appear in the catalog and about 80 percent of the objects below 300 km were unknowns [Kessler, 1982b]. The limits of the tuned radar is also shown in Figure 2.1-3.

Most important, the correction from 4 cm to 1 mm objects is unknown. The spatial density of objects in this size regime is small enough that impact sensors of reasonable size will not sustain enough encounters to yield reliable statistics, but are small enough that sensing from the ground appears unfeasible. Some information on the current densities can be obtained from models of the mass distribution of explosion fragments, since explosions would have been the source of such objects, but in general this would be a difficult argument to carry through with any confidence.

2.1.2 Small Objects

The problem of detection of microparticles is different than for larger objects, and has been done historically using impact sensors and passive optical detectors. These detectors have enabled NASA to produce a model for the meteoroid environment, as shown in Figure 2.1-6 [Cour-Palais, 1969].

Man-made debris in this size range would decay rather rapidly since the small particles have a large area to mass ratio. Hence, debris this size regime might be expected to

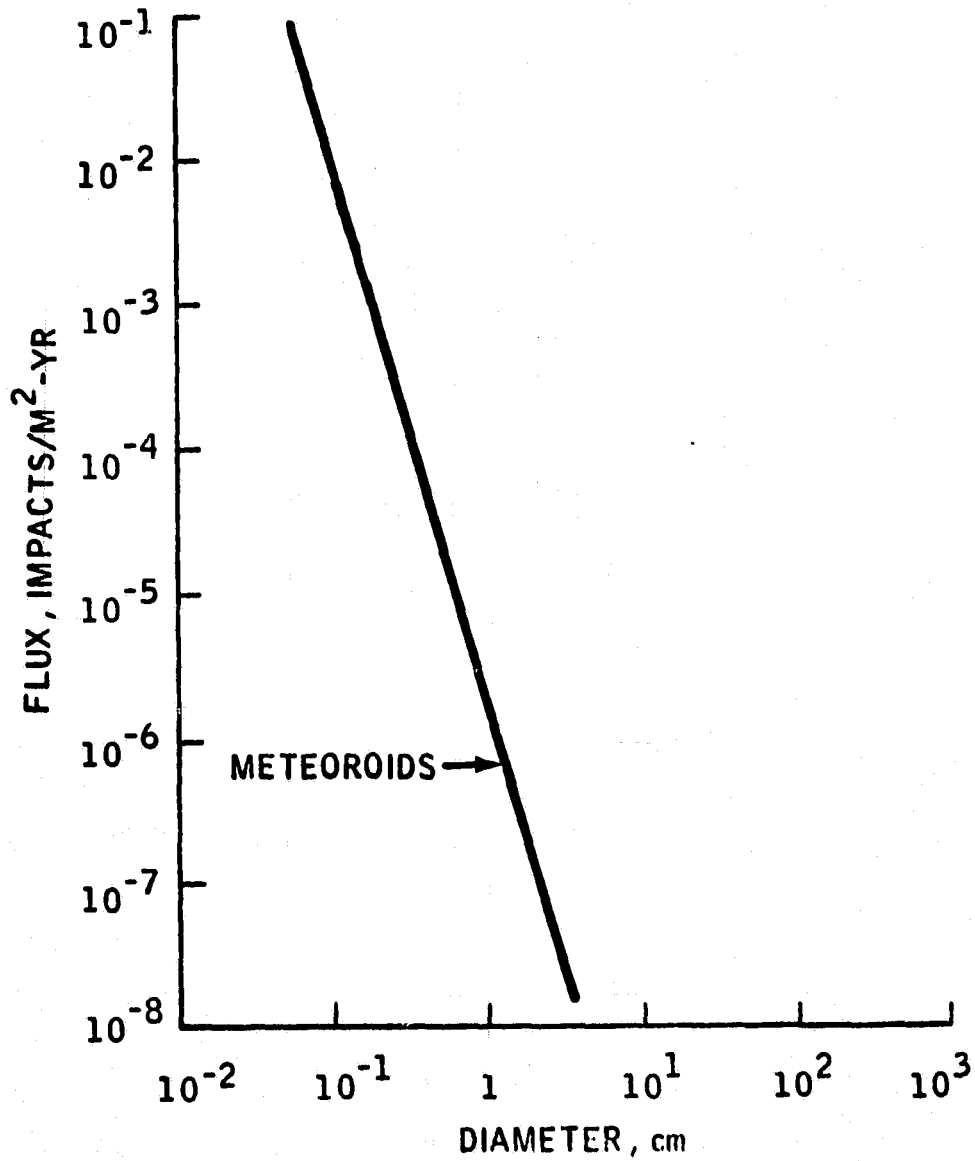


FIGURE 2.1-6. CUMULATIVE FLUX OF METEORIDS AS A FUNCTION OF MASS

exhibit a time-varying flux which would be detectable only if the sources were sufficient to significantly elevate the flux above the background. There is evidence that the man-made segment of the debris population does, in fact, dominate the meteoroid population for periods of weeks to months.

The data providing this evidence came from Explorer 46, which consisted, in part, of 2 perpendicularly oriented planar arrays of pressurized cells [Roberts, 1982]. The satellite was configured to be gravity-gradient stabilized in a mode placing one of the planar arrays in a locally horizontal orientation (the parallel array) and the other in a radial orientation (the perpendicular array). If the meteoroid velocity vectors are randomly oriented in the vicinity of the Earth, each array of cells would be expected to record the same meteoroid flux. In fact, a significantly larger flux was recorded on the perpendicular array.

One explanation for this excess would come from the firing of solid rocket motors (SRMs) in LEO during data acquisition. Particulates arising from these firings would tend to populate nearly circular orbits and so record many more impacts on the perpendicular array than on the one which was horizontal. The work of Kessler [Kessler, 1982a] revealed a correlation between SRM firings and debris flux increases, supporting this hypothesis.

The relevant data is presented in Figure 2.1-7, where the impact rates have been reduced to debris fluxes as seen by both the parallel and perpendicular surfaces. The arrows at the bottom of the graph indicate the occurrence of SRM firing. Based on the explanation given above, the elevation of the perpendicular levels is due to man-made debris, which clearly dominates the meteoroids where the spikes are seen.

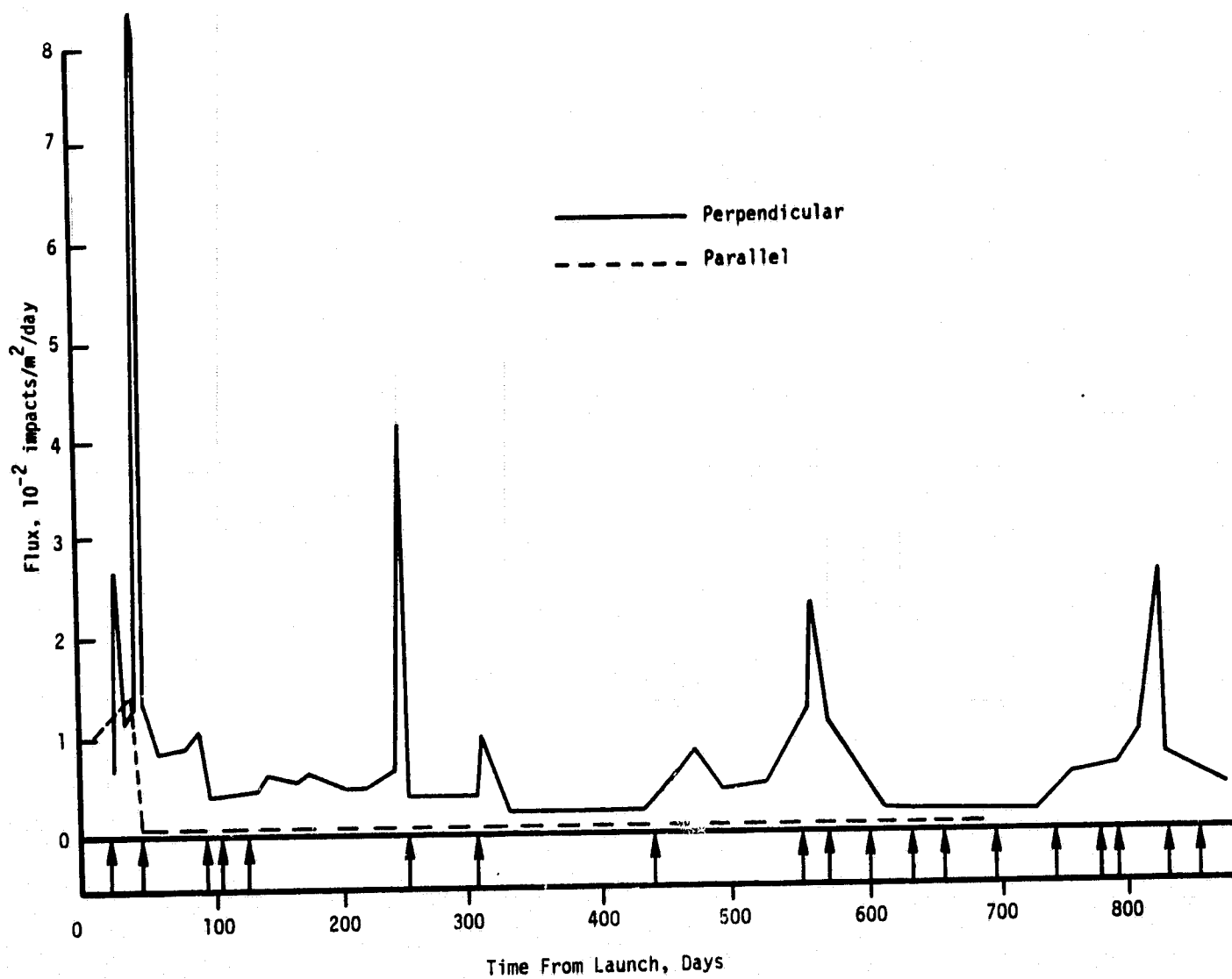


FIGURE 2.1-7. THREE IMPACT RUNNING AVERAGE FLUX FOR PERPENDICULAR AND PARALLEL SURFACES [Kessler, 1982a]

2.2 PROJECTED HAZARD LEVELS

2.2.1 Large Objects

To assess the impact of future states of the large debris population on spacecraft design, future flux levels must be determined. Nearly as important, however, is the uncertainty in this level, since the maximum sized object which must be protected against may depend rather sensitively on the actual debris flux.

The knowledge of future population states, of course, requires evolutionary models. Evolution modeling has been conducted at JSC and at Battelle's Columbus Laboratories (BCL) using different approaches. Kessler [1981, 1982] has produced future population states using an expected collision frequency, along with a calculation of mass distribution consistent with Bess [1975]. His prediction of the 1995 debris flux level is provided in Figure 2.2-1.

The BCL model has been developed using a Monte Carlo approach for the environment evolution [Reynolds et al, 1982]. The model currently lacks as much detailed information on the mass distribution of the debris as appears in the Kessler model but incorporates more information on the specific deposition properties. Results of modeling for nominal debris evolution is presented in Figure 2.2-2, 2.2-3, and 2.2-4 for a 20 year period.

In discussing projected hazard levels for the large debris, it must be recognized that uncertainty in these levels is an essential and important part of the analysis. A primary source of uncertainty is the contribution from future debris sources, since these sources will introduce debris into the environment stochastically in time and spatial location and in the detailed deposition properties. The source contribution is a major source of uncertainty because individual deposition events

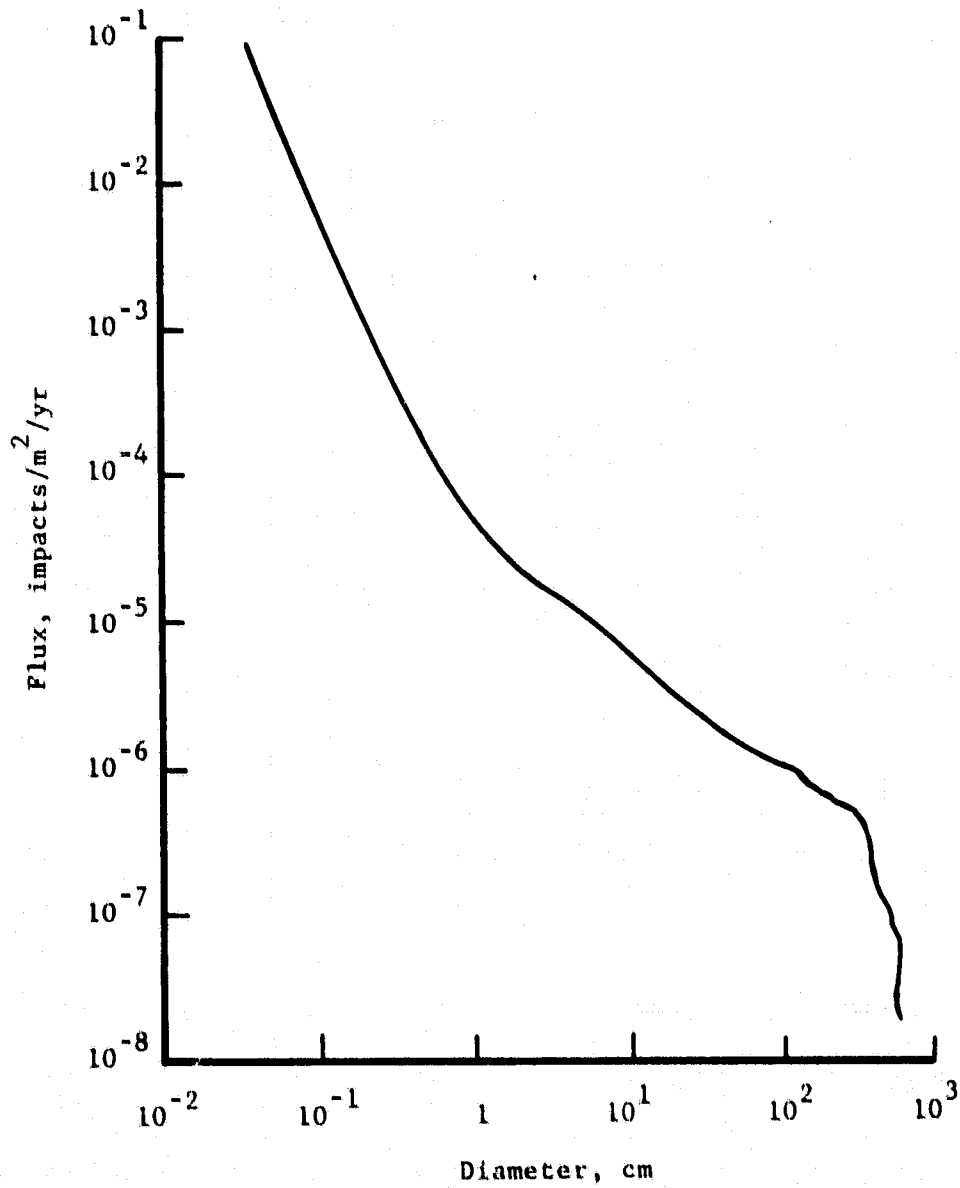
ORIGINAL PAGE IS
OF POOR QUALITY

FIGURE 2.2-1. CUMULATIVE FLUX OF MAN-MADE DEBRIS AS A FUNCTION OF SIZE FOR THE PROJECTED 1995 POPULATION

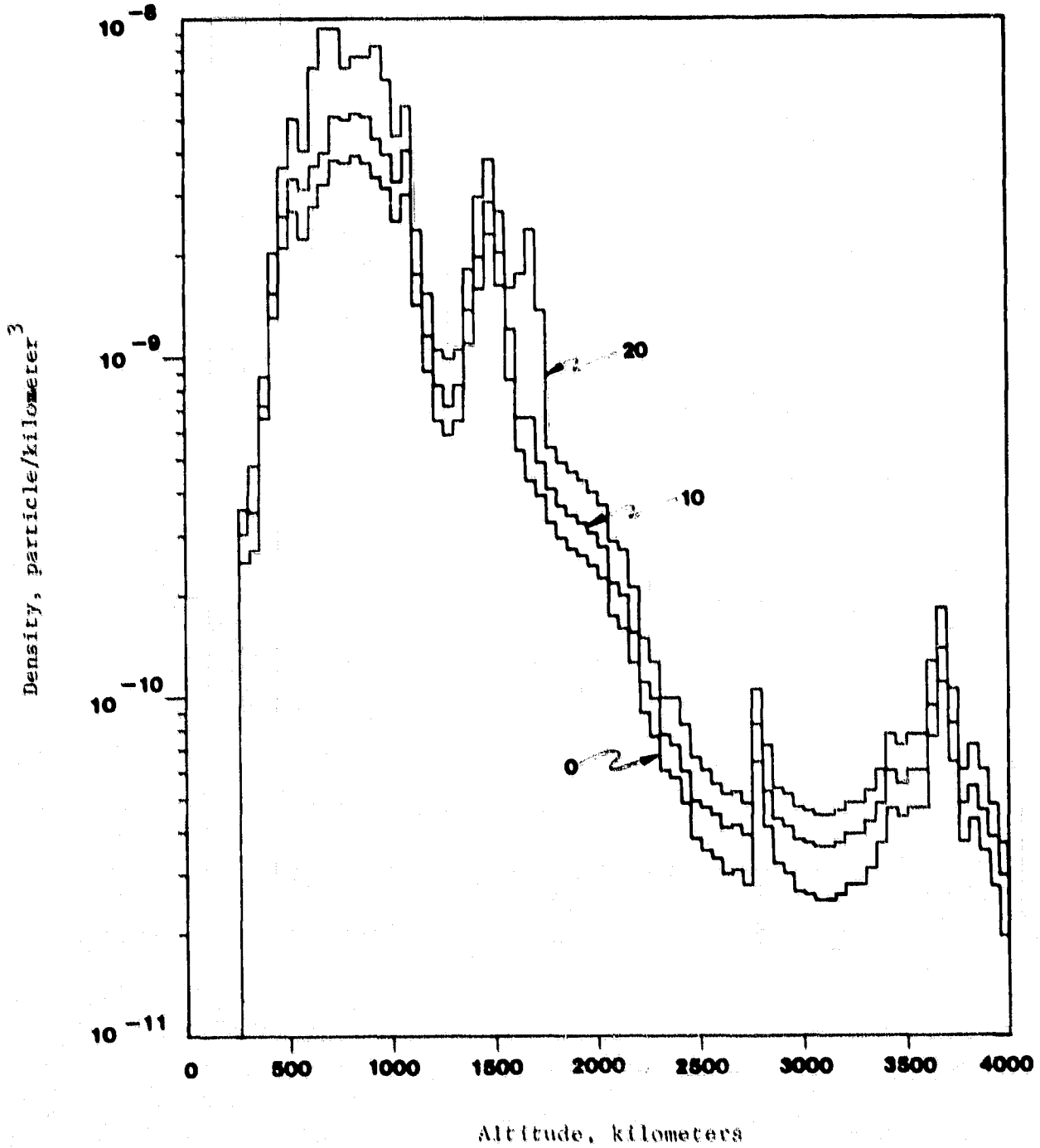


FIGURE 2.2-2. PROJECTED DEBRIS DENSITIES FOR 10- and 20-YEAR PERIODS OF EVOLUTION

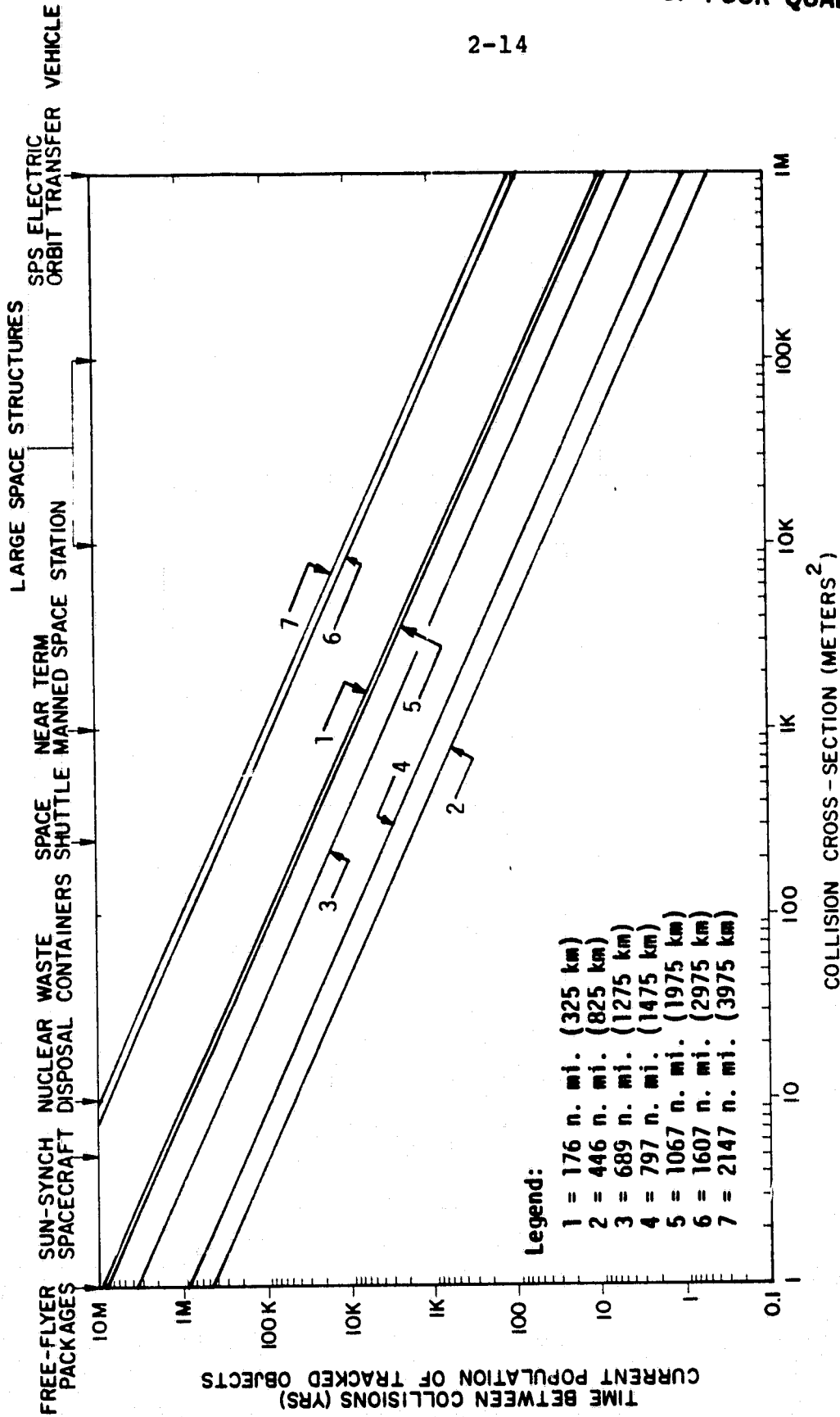


FIGURE 2.2-3. EXPECTED TIME BETWEEN COLLISIONS AS A FUNCTION OF COLLISION CROSS-SECTION FOR A PROJECTED 10-YEAR POPULATION

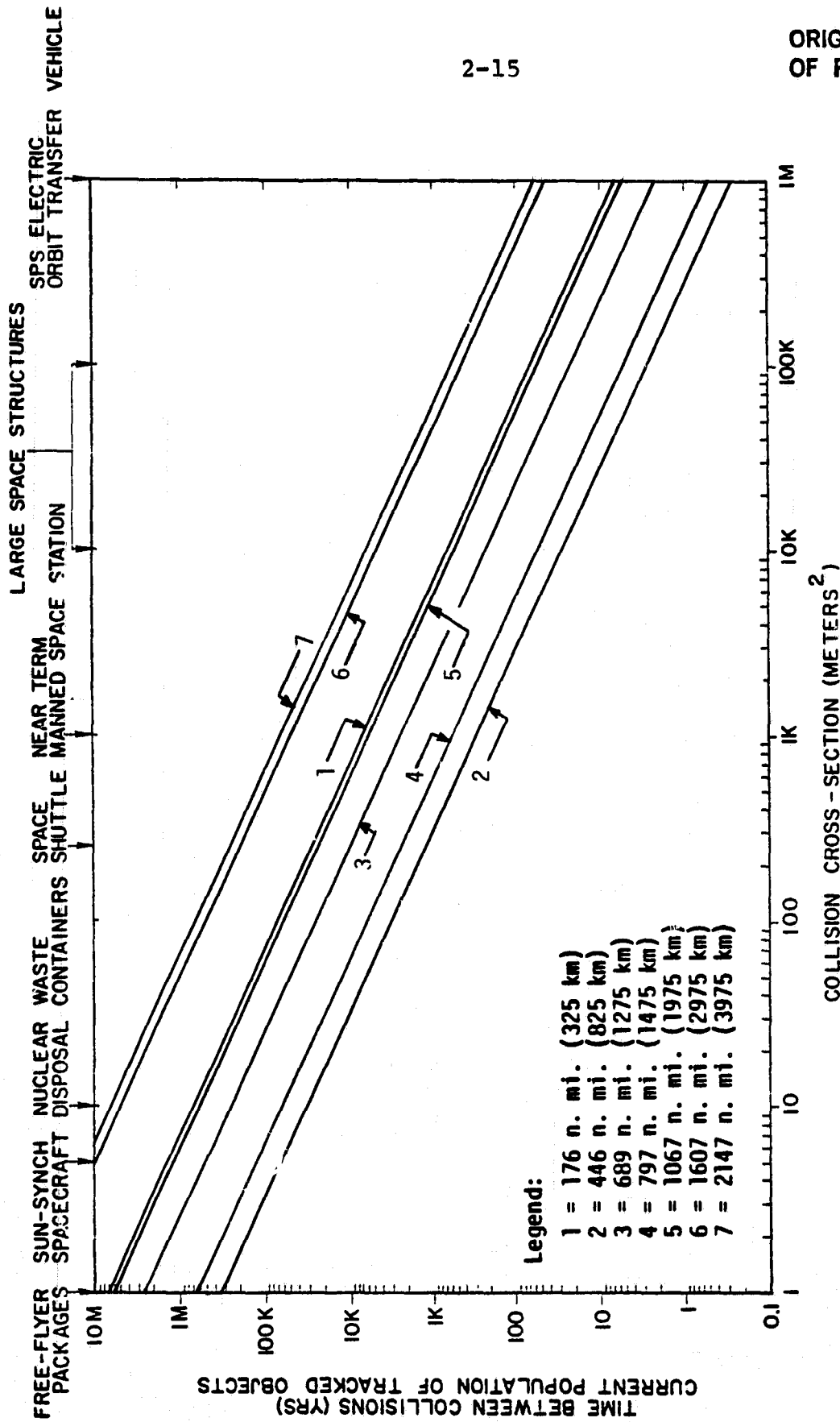


FIGURE 2.2-4. EXPECTED TIME BETWEEN COLLISIONS AS A FUNCTION OF COLLISION CROSS-SECTION FOR A PROJECTED 20-YEAR POPULATION

can radically alter the hazard level in a particular region. Even the mean rates for events such as deposition during normal operations is not known with certainty ahead of time.

The unobserved component of the debris population may also be a source of considerable uncertainty, depending on the time scale for the projection and the state of the zero-time population. This sensitivity can be shown more explicitly in the following rather simple model for the debris evolution.

The conservation of particle number requires that

$$\frac{dn}{dt} + \nabla \cdot n\vec{u} = s \quad (2.2-1)$$

where

$$\begin{aligned} n &= \text{number density (cm}^{-3}\text{)} \\ \vec{u} &= \text{population flow velocity (cm/sec)} \\ s &= \text{source term (cm}^{-3}\text{ sec}^{-1}\text{)} \end{aligned}$$

For the debris problem, \vec{u} will be the infall velocity arising from atmospheric drag. Except at lowest altitudes this will be small and can be ignored.

If the debris is divided into two classes - that which is large enough to be detected (1) and that which is small enough to escape detection with current detectors (2), a plausible form for the differential equation governing the evolution of these two subpopulations would be

$$\dot{n}_1 = k_{11} n_1 + k_{12} n_2 \equiv k_1 n_1 \quad (2.2-2a)$$

where

$$k_{11} = \text{constant measuring the contribution from normal operations}$$

k_{12} = constant measuring the contribution from explosions

$$\dot{n}_1 = \frac{dn_1}{dt}$$

and

$$\dot{n}_2 = k_{22} n_1 + k_{23} n_1 n_2 \quad (2.2-2b)$$

where

k_{22} = constant measuring the contribution from explosions

k_{23} = constant measuring the contribution from collisions

The solution to this set of differential equations is

$$n_1(t) = n_1^0 e^{k_1 t} \quad (2.2-3a)$$

$$n_2(t) = n_2^0 e^{k_2 (e^{k_1 t} - 1)} + \alpha (e^{k_2 (e^{k_1 t} - 1)} - 1) \quad (2.2-3b)$$

where

$$n_1^0 = n_1(0)$$

$$n_2^0 = n_2(0)$$

$$\alpha = k_{22}/k_{23}$$

$$k_2 = k_{23} n_1^0 / k_1$$

The number density representing a hazard to spacecraft is of course

$$n(t) = n_1(t) + n_2(t) \quad (2.2-4)$$

The first term in the expression for $n_2(t)$ is the contribution arising from the zero-time population. If $n_2(t) > n_1(t)$ and if the first term dominates or is comparable to the second term, knowledge of $n_2(0)$ would be important for future spacecraft design; if the second term dominates or if $n_2(t) \ll n_1(t)$, knowledge of $n_2(0)$ would be relatively unimportant. Although the issue cannot be resolved for the current population, arguments can be advanced for some bounding of the parameters.

Consider the expression for $n_2(t)$. Clearly for large times

$$n_2(t) \rightarrow (n_2^0 + \alpha) e^{k_2 t} e^{k_1 t}$$

so that $n_1(t) \ll n_2(t)$ and dominance of terms depends solely on n_2^0/c . At other times, some insight into the relative importance of terms can be obtained by bounding the coefficients. We have

$$k_1 \approx 0.05 \text{ yr}^{-1}$$

with

$$k_{11} \approx k_{12} \approx 0.025 \text{ yr}^{-1}$$

k_{22} can be related to k_{12} ; it is in the range of 1+1000 times k_{12} .

$$k_{22} \approx 0.025 + 25 \text{ yr}^{-1}$$

$$k_{23} = \bar{\sigma} v_R n_c$$

where

$$n_c = \text{number of objects generated in collision}$$

$$k_{23} = 10^4 \cdot 10^6 \cdot 10^{4+6} = 10^{14+16} \text{ sec}^{-1} = 10^{21+23} \text{ yr}^{-1}$$

$$\alpha = \frac{.025+25}{10^{21+23}} = 2.5 \times 10^{-20+-25}$$

$$k_2 = \frac{10^{21+23} \cdot 10^{-8+-10} \cdot 10^{-15}}{.05} = .02+20$$

$$n_2^0 = 10^{-8+-10} \cdot 10^{-15} = 10^{-23+-25}$$

so that

$$n_2(t_y) = 10^{-23+-25} e^{(.02+20)t_y} (e^{.05t_y} - 1) + 2.5 \times 10^{-20+-25} (e^{(.02+20)t_y} (e^{.05t_y} - 1) - 1) \quad (2.2-5)$$

where t_y is time in years.

The equivalent expression for $n_1(t)$ is simply

$$n_1(t_y) = 10^{-23+-26} e^{0.5t_y} \quad (2.2-6)$$

In assessing the dominant terms in the expression for $n(t)$, the important terms in Equations 2.2-5 and 2.2-6 are evaluated in Table 2.2-1. Clearly, the parameter which is most critical in determining the dominant term is k_2 which is driven by k_{23} , which is driven by n_c . With the current uncertainties in parameter values, the importance of $n_2(t)$ cannot be determined for the current population.

TABLE 2.2-1. VALUES OF THE IMPORTANT TERMS IN EXPRESSIONS 2.2-5,6

ty	$e^{.05ty}$	$e^{.02} (e^{.05ty} - 1)$	$e^2 (e^{.05ty} - 1)$	$e^{20} (e^{.05ty} - 1)$
1	1.05	1.01	1.11	2.79
5	1.28	1.05	1.76	2.93
10	1.65	1.14	3.66	4.3×10^5
20	2.72	1.41	31.08	8.4×10^{14}

A second effect on the sensitivity of spacecraft design to uncertainties in the debris flux involves the mass spectrum in the vicinity of the mass value of concern. If the cumulative flux is increasing rapidly in this region, the mass uncertainty is less for a given flux uncertainty than if it is increasing more slowly. The relationship between Δm , the uncertainty in the mass value of concern, Δf , the uncertainty in the cumulative flux, and $f' = df/dm$, for small uncertainties in the cumulative flux, will be

$$\Delta m = \frac{\Delta f}{f'}$$

f' would be expected to be low at low altitude, where the small debris will be dragged out, and large at high altitude, where the power law mass distribution is maintained for a longer time. A plot showing this effect is presented in Fig. 2.2-5 [Kessler, 1982a] for Kessler's 1995 reference population.

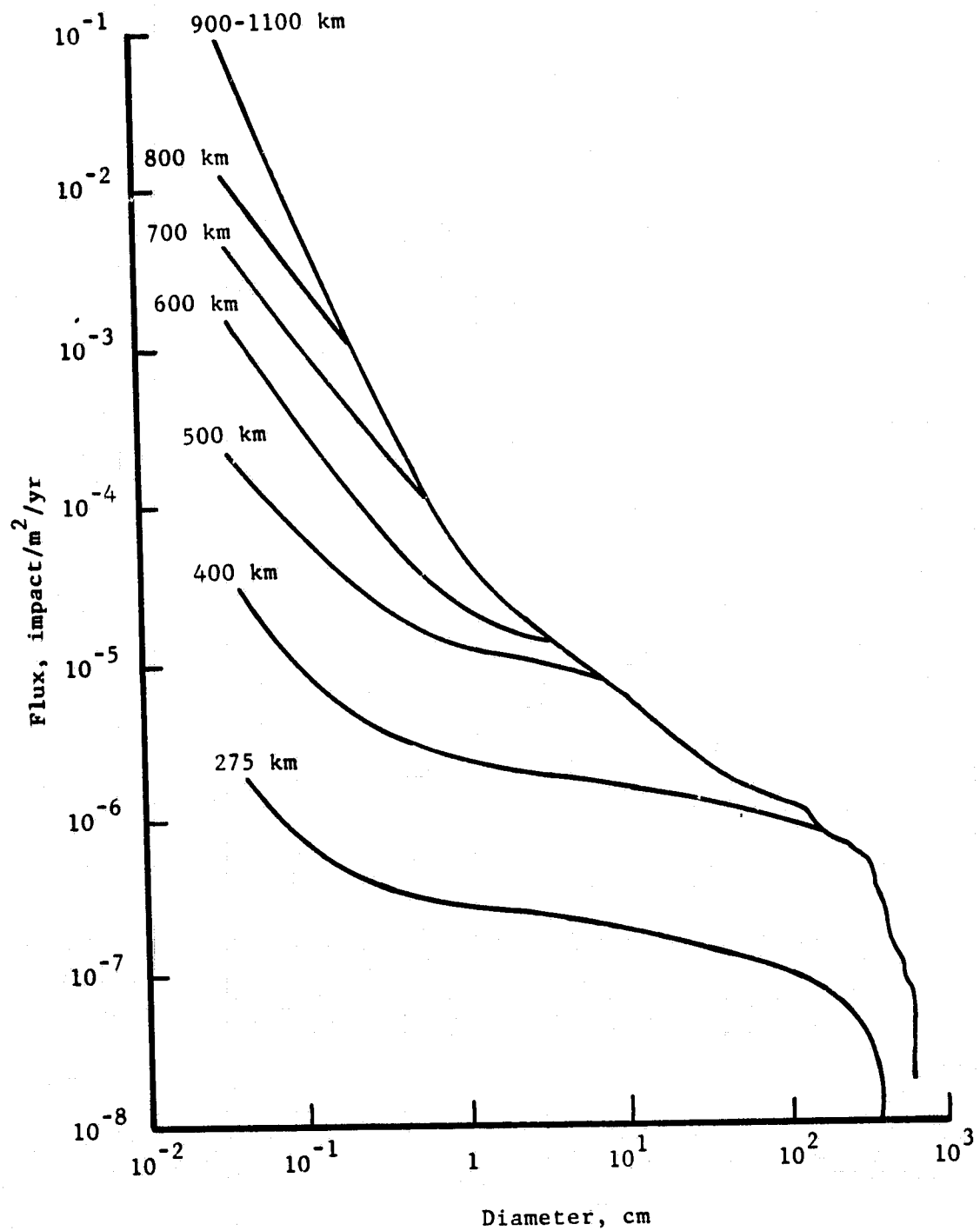
ORIGINAL PAGE IS
OF POOR QUALITY

Figure 2.2-5. PREDICTED 1995 CUMULATIVE DEBRIS FLUX LEVELS FOR A SET OF ALTITUDES [Kessler, 1982a]

These cumulative flux plots can be used to obtain a set of sample values to illustrate this effect. Expressed in the figure variables,

$$\frac{1}{3} \frac{\Delta m}{m} = \frac{\Delta r}{r} = \frac{\Delta \ln f}{g'}$$

where

$$g' = d(\ln f)/d(\ln r).$$

g' is the slope of the tangent line at a point on the cumulative flux plots. For the 275 km population, assuming a particle density of 3 gm/cm³, the results are presented in Table 2.2-2.

TABLE 2.2-2. UNCERTAINTIES IN THE DEBRIS MASS OF CONCERN AS FUNCTION OF DEBRIS SIZE FOR A 5 PERCENT UNCERTAINTY IN THE CUMULATIVE FLUX. CUMULATIVE FLUX DISTRIBUTION FOR 275 Km.

m (gm)	r (cm)	g'	r (cm)	m (gm)
.0126	0.1	0.84	0.006	2.2×10^{-3}
12.6	1.0	0.13	0.380	14.4
12.6×10^3	10.0	0.20	2.46	9.29×10^3

A similar table can be generated to show the variation of the mass uncertainty at a given mass value at the various altitudes. Again, for a 5 percent flux uncertainty, for a 1 cm sized object, Table 2.2-3 provides the uncertainties as a function of altitude for the population of Fig. 2.2-5.

TABLE 2.2-3. UNCERTAINTY IN THE DEBRIS MASS OF CONCERN AS A FUNCTION OF ALTITUDE FOR A 5 PERCENT UNCERTAINTY IN THE DEBRIS FLUX

h	g'	m(gm)
275	0.13	14.4
400	0.27	7.05
600	0.62	3.02
700-1100	1.38	1.32

From the range of values shown in these two tables, it is obvious that the behavior of the cumulative flux distribution in the neighborhood of the mass concern to spacecraft designers will have some impact on their concern for population uncertainties.

2.2.2 Small Objects

In projecting the small object population, the two sources presenting the greatest potential contribution are the SRM firings and collisions between objects on orbit. As was noted in the last section, there is considerable uncertainty in when collisions will become a common occurrence; furthermore, the expected number of objects in this size range is not a well-defined quantity. Much better data is available on SRM exhaust particulates and this source promises to inject an immense number of particles into the environment. Therefore, in the following discussion, only this source will be considered.

A model for the size distribution of particulates in the Inertial Upper Stage (IUS) plume is presented in Fig. 2.2-6 [Roberts, 1982] and provided in Table 2.2-4.

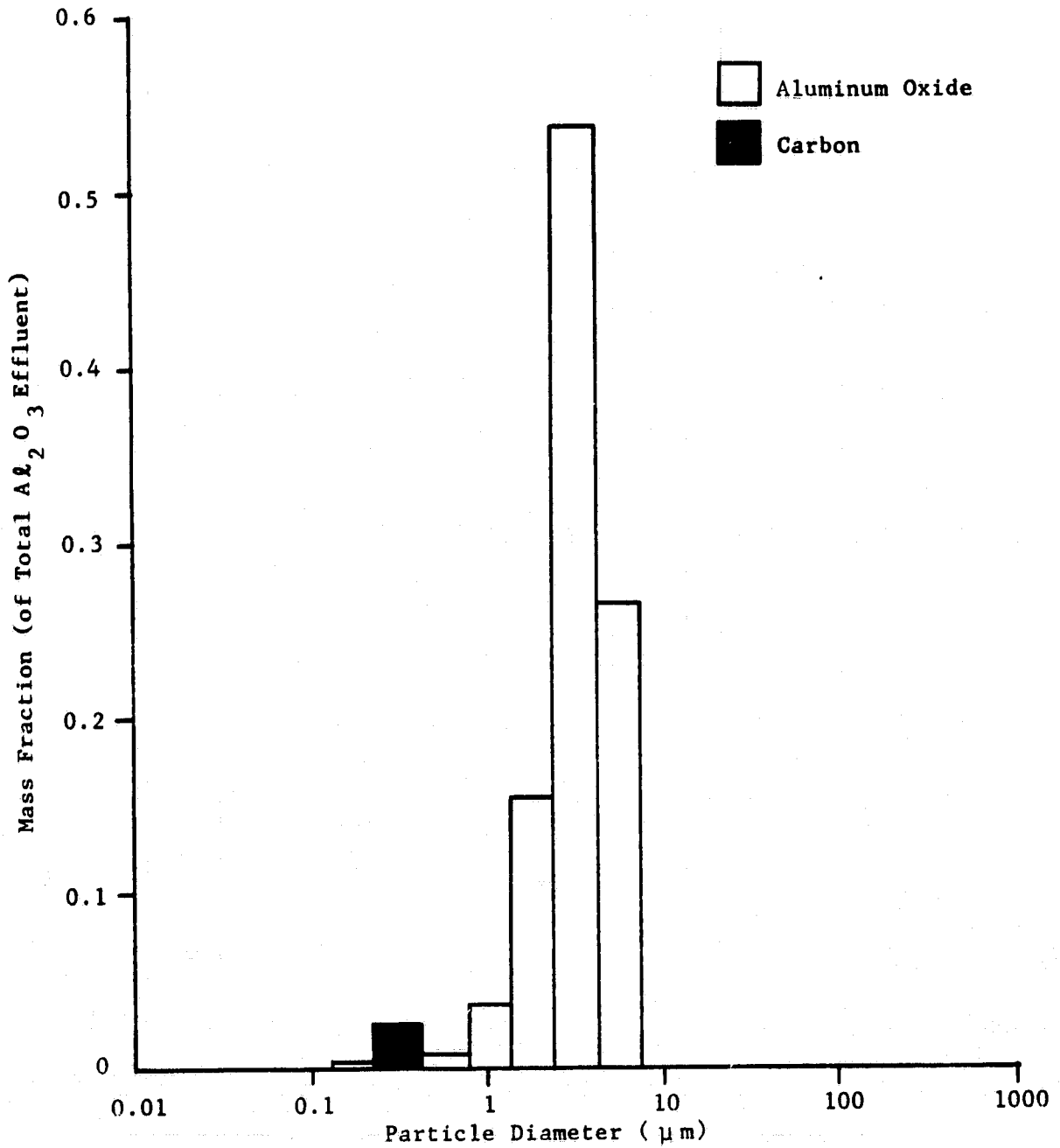


FIGURE 2.2-6. A MODEL FOR THE SIZE DISTRIBUTION OF PARTICULATES IN THE INERTIAL UPPER STATE (IUS) PLUME [Roberts, 1982]

TABLE 2.2-4. YEARLY CONTRIBUTION OF SRM PARTICULATES INTO LEO FOR 3 MISSION MODELS [Roberts, 1982]

Mission Model	Number of Flights/Year	SUSS-A	SUSS-D	IUS	Total (lbs)
Low	24	9,560	20,735	24,708	55,002
Nominal	40	15,934	34,558	41,153	91,645
High	60	23,901	51,836	61,770	137,507

If the IUS mass distribution is assumed for both the SUSS-A and SUSS-D, the number of particles injected into the environment each year by solid rockets can be calculated. For a mass-weighted mean diameter of 4 μm the numbers are as shown in Table 2.2-5. If all of these particles were to remain in orbit, they would produce a flux of about $1/\text{m}^2/\text{sec}$.

TABLE 2.2-5. NUMBER OF SRM PARTICULATES INTRODUCED ANNUALLY INTO LEO FOR 3 MISSION MODELS

Mission Model	Total Weight (lbs)	Number of Particulates
Low	55,002	1.5×10^{17}
Nominal	91,645	2.5×10^{17}
High	137,507	3.7×10^{17}

Fortunately, a vast preponderance of these particulates will be removed very quickly. An estimate of the future flux can be obtained by scaling the Explorer 46 data to account for the

enhanced SRM activity. Table 2.2-6 presents the required information.

TABLE 2.2-6. EXPLORER 46 DATA NEEDED TO ESTABLISH
MAN-MADE DEBRIS FLUX LEVELS
(IMPACTS/METER²/DAY)

Plane	Average Area (m ²)	Number of Impacts (900 days)	Mean Flux (m ⁻² d ⁻¹)
Parallel	5.0	8	.0018
Perpendicular	9.0	43	.0053

The mean flux from man-made debris is therefore 0.0035 m⁻²d⁻¹. During this 900 day period there were 19 SRM firings, for an annual rate of 7.7. Factoring these rates together yields fluxes for the 3 models as presented in Table 2.2-7. Based on Fig. 2.1-7, a more involved analysis of the data might show that the flux exceeds the mean by a factor of 10 a significant percentage of time.

TABLE 2.2-7. PROJECTED SRM PARTICULATES FLUXES
FOR 3 MISSION MODELS

Mission Model	Number of Flights/Year	Flux (m ⁻² d ⁻¹)	Flux (m ⁻² yr ⁻¹)
Low	24	.011	4.0
Nominal	40	.018	6.6
High	60	.027	10.0

2.3 DEFINITION OF REFERENCE POPULATIONS

The projected debris hazard discussed in the previous section can be used to define reference debris flux levels. Table 2.3-1 presents the 10- and 20-year flux levels (f_{cons}^{10} and f_{cons}^{20}) from the BCL model, and the 1-mm and 1-cm cumulative flux levels (f_{lmm}^{1995} and f_{lcm}^{1995}) from the JSC model. A plot of flux levels versus altitude is presented in Figure 2.3-1. There are significant discrepancies between f_{cons}^{20} and f_{lmm}^{1995} , and these fluxes should be comparable.

TABLE 2.3-1. DEBRIS FLUX ($\text{M}^{-2} \text{YR}^{-1}$) AS A FUNCTION OF ALTITUDE FOR THREE REFERENCE POPULATION MODELS

h (km)	f_{cons}^{10}	f_{cons}^{20}	f_{lcm}^{1995}	f_{lmm}^{1995}
275	9.8×10^{-8}	1.4×10^{-7}	3.3×10^{-7}	7.5×10^{-7}
400	4.3×10^{-7}	5.7×10^{-7}	2.4×10^{-6}	1.0×10^{-5}
500	1.2×10^{-6}	1.8×10^{-6}	1.3×10^{-5}	6.5×10^{-5}
600	1.4×10^{-6}	2.2×10^{-6}	2.3×10^{-5}	6.7×10^{-4}
700	1.8×10^{-6}	3.7×10^{-6}	5.2×10^{-5}	1.2×10^{-3}
800	2.0×10^{-6}	2.4×10^{-6}	5.2×10^{-5}	3.2×10^{-3}
1000	1.4×10^{-6}	2.1×10^{-6}	5.2×10^{-5}	7.3×10^{-3}

The BCL fluxes provide a conservative (hence f_{cons}) prediction of the debris flux levels. The growth in the large debris of 5% per year is not a conservative level of expected growth, but only the tracked population was used for the

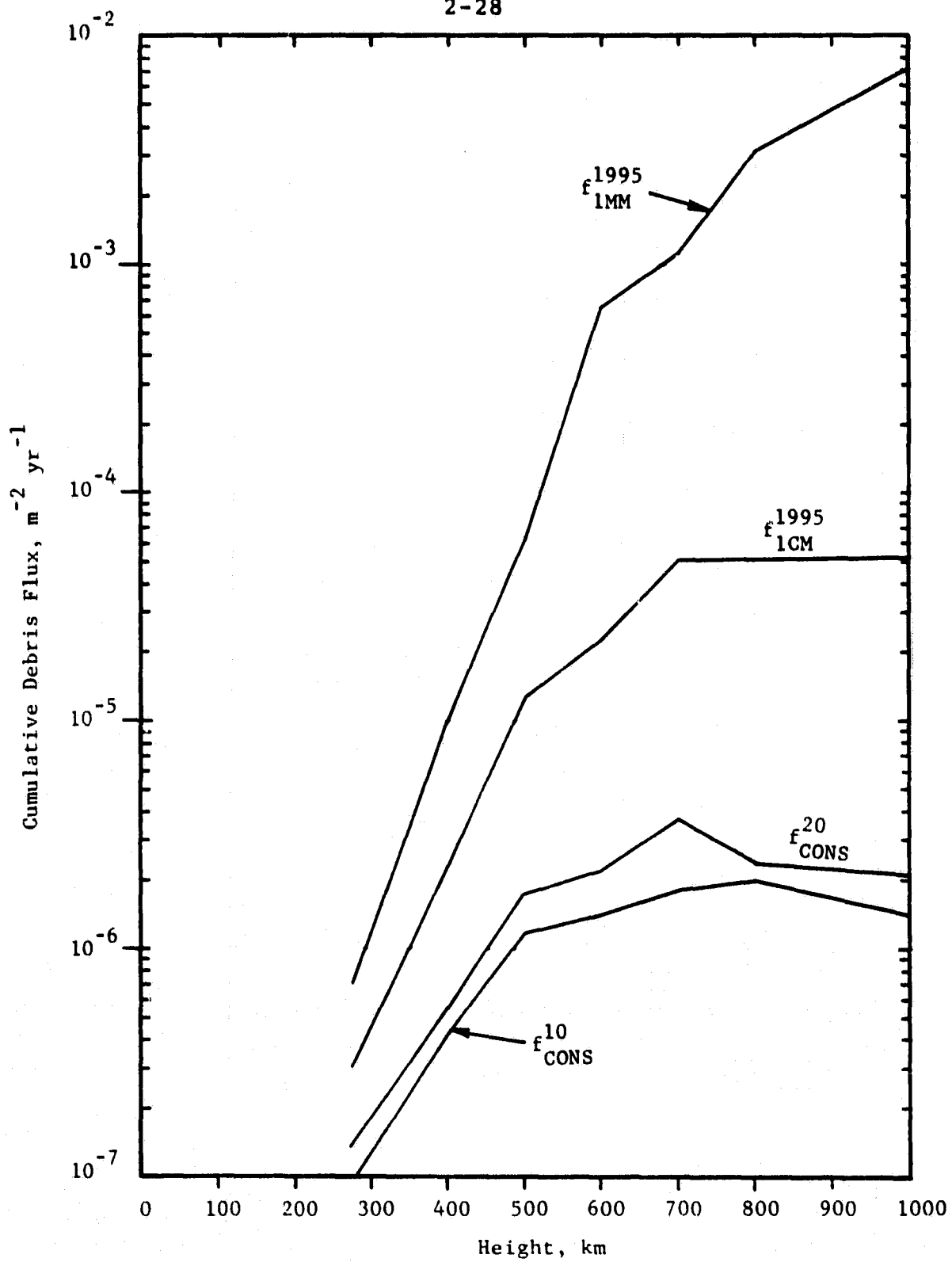


FIGURE 2.3-1. DEBRIS FLUX AS A FUNCTION OF ALTITUDE FOR THREE REFERENCE POPULATIONS

zero-time population - no correction was made for unobservable objects. The typical time to first collision was in the 16-17 year time frame [Reynolds et al, 1982].

The JSC fluxes are less conservative because a correction was made for unobservable objects, contributions from accidental explosions were included, and a collision frequency of 1 collision per 3 years was adopted [Kessler, 1982].

Neither set of fluxes took into account fragments produced in ASAT tests, so both fluxes will be conservative in an era of schrapnel producing ASAT testing.

There are two sources which probably account for the discrepancy in projected fluxes. Besides including a correction factor for unobserved objects, the JSC zero-time population consists of objects which are somewhat larger than the zero-time BCL population. In particular, the objects in the BCL middle-sized category, which have a characteristic diameter of about 6", should have a size more nearly 30" to be in better agreement with JSC. Both effects, if included in additional BCL modeling, would produce larger projected fluxes.

2.4 DETECTION RANGES

Detection ranges can be determined using the reference population fluxes provided in Table 2.3-1 along with a desired detection frequency. Detection ranges for 10 and 100 detection events per year were established.

Active Detectors

An active, gated detector will scan a portion of a spherical surface of radius $R_d = ct_d$, where t_d is the time between transmission and reception, c the speed of light. The area scanned will depend on the delay time, t_d , as well as on the

ORIGINAL PAGE IS
OF POOR QUALITY

detector cone half-angle, α . The geometry is shown in Fig. 2.4-1. The effective area for measuring impact rates will be the base area of the cone,

$$A_d = \pi(R_d \sin\alpha)^2 \quad (2.4-1)$$

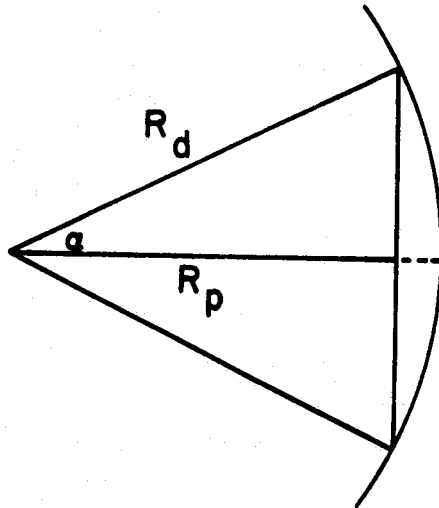


FIGURE 2.4-1. GEOMETRY FOR DETERMINING DETECTOR CAPABILITIES

To achieve a given detection area, there is a trade-off between the cone angle, which places demands on the scanning electronics as well as radiated power, and the range, which places demands on the radiated power.

If the axis of the cone is pointed along the flux vector, the relationship between the number of detection events, N , flux f , and A_d is

$$N = A_d f = \pi f (R_d \sin \alpha)^2 \quad (2.4-2)$$

or

$$R_d = \sqrt{\frac{N}{\pi f \sin^2 \alpha}} \quad (2.4-3)$$

The ranges required for the reference fluxes of Table 2.3-1 are presented in Table 2.4-1 for both 10 and 100 detection events per year.

TABLE 2.4-1. DETECTION RANGE (KM) FOR 10 (100) EVENTS PER YEAR AS A FUNCTION OF ALTITUDE (DETECTOR CONE ANGLE = 60°)

h	10 R_{cons}	20 R_{cons}	1995 R_{1cm}	1995 R_{1mm}
275	11.4 (36.0)	9.5 (30.2)	6.2 (19.6)	4.1 (13.0)
400	5.4 (17.2)	4.7 (14.9)	2.3 (7.3)	1.1 (3.6)
500	3.3 (10.3)	2.7 (8.4)	0.99 (3.1)	0.44 (1.4)
600	3.0 (9.5)	2.4 (7.6)	0.74 (2.4)	0.14 (0.44)
700	2.7 (8.4)	1.9 (5.9)	0.49 (1.6)	0.10 (0.33)
800	2.5 (8.0)	2.3 (7.3)	0.49 (1.6)	0.06 (0.20)
1000	3.0 (9.5)	2.5 (7.8)	0.49 (1.6)	0.04 (0.13)

Passive Detectors

For a passive detector pointing along the direction of the velocity vector, the same arguments apply as above. However, for a detector pointing away from the direction of motion, as is the IRAS instrument, the volume of the cone which the detector is scanning is the quantity which must be considered. A detection frequency can be related to the expected number of objects in the field of view and the expected time spent crossing the field of view. In particular

$$D = \frac{\langle N \rangle}{\langle t_c \rangle} \quad (2.4-4)$$

where

$\langle N \rangle$ = expected number of objects in the field of view
 $\langle t_c \rangle$ = expected time crossing the field of view

The expression for $\langle N \rangle$ is simply

$$\langle N \rangle = n \cdot \text{volume of cone} = \frac{1}{3} \pi R_p^3 (\tan \alpha)^2 n \quad (2.4-5)$$

where

n = number density

To get an expression for the expected time an object will remain in the cone, the expected transverse distance speed must be considered. This can be done relatively easily if the cone axis is nearly radial and the debris motion is nearly circular. The expected length for a randomly chosen chord cutting a circle of radius R is $\pi R/2$. An expression for $\langle t_c \rangle$ is then

$$\langle t_c \rangle = \frac{\int_0^{R_p} \frac{\pi r \tan \alpha}{2 v_t} \cdot \pi r^2 \tan^2 \alpha \, dr}{\int_0^{R_p} \pi r^2 \tan^2 \alpha \, dr} \quad (2.4-6)$$

or

$$\langle t_c \rangle = \frac{3\pi}{8} \frac{R_p \tan \alpha}{v_t} \quad (2.4-7)$$

Therefore

$$D = \frac{\frac{\pi}{3} R_p^2 (\tan \alpha)^2 n}{\frac{3\pi}{8} \frac{R_p \tan \alpha}{v_t}} \quad (2.4-8)$$

or

$$D = \frac{8}{9} v_t n R_p^2 \tan \alpha \, (\text{sec}^{-1}) \quad (2.4-9)$$

or

$$D_y = 2.8 \times 10^7 v_t n R_p^2 \tan \alpha \, (\text{year}^{-1}) \quad (2.4-10)$$

and the expression for the range becomes

$$R_p = \sqrt{\frac{3.6 \times 10^{-8} D_y}{v_t n \tan \alpha}} \quad (2.4-11)$$

where R_p is in the same units as v_t and n . A table of n values for the reference populations is presented in Table 2.4-2. Adopting a value of 7 km/sec for v_t and 2° for α , the detection distances for 10 and 100 detections per year are provided in Table 2.4-3.

TABLE 2.4-2. DEBRIS DENSITY (KM^{-3}) AS A FUNCTION OF ALTITUDE FOR THREE REFERENCE POPULATION MODELS

h (km)	10 n_{cons}	20 n_{cons}	1995 $n_{1\text{cm}}$	1995 $n_{1\text{mm}}$
275	4.6×10^{-10}	6.5×10^{-10}	1.5×10^{-9}	3.5×10^{-9}
400	2.0×10^{-9}	2.7×10^{-9}	1.1×10^{-8}	4.7×10^{-8}
500	5.6×10^{-9}	8.4×10^{-9}	6.0×10^{-8}	3.0×10^{-7}
600	6.5×10^{-9}	1.0×10^{-8}	1.1×10^{-7}	3.1×10^{-6}
700	8.4×10^{-9}	1.7×10^{-8}	2.4×10^{-7}	5.6×10^{-6}
800	9.3×10^{-9}	1.1×10^{-8}	2.4×10^{-7}	1.5×10^{-5}
1000	6.6×10^{-9}	9.7×10^{-9}	2.4×10^{-7}	3.4×10^{-5}

TABLE 2.4-3 PASSIVE DETECTION RANGE (KM) FOR 10 (100) EVENTS PER YEAR WITH A CONE ANGLE OF 4°

h (Km)	10 R_{cons}	20 R_{cons}	1995 $R_{1\text{cm}}$	1995 $R_{1\text{mm}}$
275	56.3 (178)	47.4 (150)	31.2 (98.7)	20.4 (64.6)
400	27.0 (85.4)	23.3 (73.5)	11.5 (36.4)	5.6 (17.6)
500	16.1 (51.1)	13.2 (41.7)	4.9 (15.6)	2.2 (7.0)
600	15.0 (47.4)	12.1 (38.2)	3.6 (11.5)	0.69 (2.2)
700	13.2 (41.7)	9.3 (29.3)	2.5 (7.8)	0.51 (1.6)
800	12.5 (39.6)	11.5 (36.4)	2.5 (7.8)	0.31 (0.99)
1000	14.9 (47.0)	12.3 (38.8)	2.5 (7.8)	0.21 (0.66)

3.0 DETECTOR SYSTEMS--LARGE PARTICLES

ORIGINAL PAGE IS
OF POOR QUALITY

3.1 GROUND-BASED SYSTEMS

3.1.1 Radar Systems

The question as to the potential ability of existing ground based radar systems to contribute to the determination of the debris particle population in the smaller size ranges cannot be answered unequivocally, in general, without recourse to classified performance data on the radar systems. Of the radars which contribute to the NORAD tracking capability, the system having the greatest capability is the PARCS radar located in North Dakota. This radar was originally intended as a test bed prototype acquisition radar for an ABM defense system.

The actual performance parameters of this radar are classified; however, some estimates of its performance can be generated using unclassified information. All existing high power radars operate at frequencies of the order of 10 GHz and below. Most operate in the 500 MHz to 3 GHz range. At these frequencies, particles with diameters of 10 cm and below are Rayleigh scatters. The radar cross section of a spherical metal particle in the Rayleigh region is:

$$\sigma = 9\pi k_o^4 a^6 \quad (3.1-1)$$

where $k_o = \frac{2\pi}{\lambda}$, λ the radar wavelength, and a is the particle radius.

For an arbitrarily shaped metallic particle, the Rayleigh radar cross section is:

$$\sigma = \frac{4}{\pi} k_o^4 V^2 \left[1 + \frac{e^{-V}}{\pi V} \right]^2 \quad (3.1-2)$$

where V is the particle volume, and v is a characteristic of the particle aspect ratio.

If the PARCS radar can detect a "vollyball" at 1200 nmi and we can assume a "vollyball" has a 10 cm radius, then the detection range for smaller sized particles reduces quite rapidly. The NORAD PARCS small satellite tests indicate detection limits of the order of 4 cm diameter particles at about 400 km altitude [Kessler, 1982].

The detection range for any radar can be determined from the radar equation. This is usually presented in the form of the signal to noise ratio at the radar detector, which is

$$S/N = \frac{P_t G_t G_r \lambda^2 \sigma n L}{(4\pi)^3 R^4 k T_e B_e} \quad (3.1-3)$$

where the parameters are:

P_t = peak transmitter power

G_t = transmit antenna gain

G_r = receive antenna gain

λ = radar wavelength

σ = target radar cross section

n = number of pulses incoherently integrated

L = system losses

R = target range

k = Boltzmann constant

T_e = receiving system effective-noise temperature in°K

B_e = effective system coherent bandwidth.

For a specified detection probability and design false alarm rate, the signal to noise ratio at the detector is determined. Thus, for a particular radar such as the PARCS, all the parameters in the radar equation are constants except for the range and the target cross sections. Thus, we can write:

$$S/N = K\sigma/R^4. \quad (3.1-4)$$

Now substituting for σ gives:

$$S/N = 9\pi k_0^4 K a^6/R^4 \quad (3.1-5)$$

or

$$R^4 \propto a^6$$

or

$$R \propto a^{1.5} \quad (3.1-6)$$

This indicates that for Rayleigh scatters, the radar detection range is proportional to the particle diameter to the 3/2 power. This will be universally true for a given radar.

Estimates of the PARCS performance based on this expression and the comments on its ability to see a "volleyball sized object at 1200 nmi are consistent with the results of the small satellite tests and indicate that objects much below golf ball size cannot be seen by the PARCS except at very low altitudes.

There are no other ground radar installations which can significantly improve on the PARCS performance. Various other high power radars exist; however, to improve upon the PARCS would require a combination of higher power output, higher frequencies, or larger antennas. A number of current radars have been examined, as indicated in Table 3.1-1, and no systems currently exist which are better in this regard.

TABLE 3.1-1. GROUND RADARS EXAMINED FOR DEBRIS
DETECTION POTENTIAL

Type	Application
AN/FPS-16	Instrumentation
AN/FPQ-6	Instrumentation
AN/FPS-17	BMEW, Space Track, Intelligence
AN/FPS-49	BMEW
AN/FPS-50	BMEW
AN/FPS-85	Space Track
Cobra Dane	BMEW, Space Track, Intelligence

3.1.2 Optical Systems

Of the existing and near term optical systems, that potentially having the greatest capability for small particle debris detection is the U.S. Air Forces' GEODSS system, which is an electro-optical deep space surveillance system consisting of sites at several locations around the world with telescopes capable of "detecting soccer ball size objects at geosynchronous altitudes" [Smith, 1979]. The precise performance parameters of these devices is also classified; however since the radiated flux from an object is proportional to the area of the object, the detection range should be proportional to the diameter of the object. If a soccer ball is assumed to be about 20 cm in diameter, a 2 cm particle should be detectable at 2200 nmi and a 2 mm particle at 220 nmi by this system.

The actual detection limits of this system will also depend upon the system integration times and bandwidths. Since it is intended primarily for monitoring objects at geosynchronous

altitudes, which will exhibit relatively low angular rates within the system field of view, the actual performance for debris particle detection may depend strongly on the angular rates exhibited. Without knowledge of the classified details of the system, no judgement can be made other than that the basic system sensitivity appears adequate to detect particles of several millimeter diameter at several hundred nautical mile altitudes.

3.2 SPACE QUALIFIED SYSTEMS

3.2.1 Radar Systems

To date there are no radar systems that have been flown whose function has been particle detection. The active radar sensors flown have been altimeters on S-193, GEOS-3, SKYLAB, and SEASAT, a scatterometer on SKYLAB and SEASAT, and an imaging synthetic aperture radar (SAR) on SKYLAB, SEASAT, and the Shuttle.

None of these systems are directly suitable for a debris detection radar. The altimeter is a short pulse radar with a wide beamwidth antenna which looks at the Earth directly below the spacecraft. The scatterometer is a system which looks at several angles simultaneously and is a continuous wave (CW) system. The imaging radar generates radar images of a swath which is parallel to the spacecraft orbit and offset to the side.

Of the components used in these systems, the traveling wave tube (TWT) power amplifier and power supply used in the altimeter is the best candidate as the power amplifier for a debris detecting radar. This tube has a wide bandwidth and is capable of a peak power output of 2 kw in the frequency range from 13 to 15 GHz.

A few additional components such as the RF portions of the altimeter receiver could also potentially be used in a debris

detection radar. The remaining components of such a radar would have to be fabricated and space qualified.

3.2.2 Electro-optical System

Two experiments were carried by Pioneer 10 and 11 whose objective was to determine the nature of the particulate environment traversed by the spacecraft [Soberman, 1974]. The asteroid/meteoroid detector (AMD), or Sisyphus, was one of these. This instrument served the dual purpose of measuring the contribution to sky brightness in white light from the aggregate of particles in the field of view and measuring individual particles as they passed through the field of view if they reflected or scattered sufficient sunlight to be detected above the sky brightness background.

The detector consisted of four 20-cm aperture optical telescopes mounted at an angle of 45° with respect to the vehicle spin axis (135° to the Earth line) [Jurkevich, 1971]. The telescopes had 7.5° fields of view and were aligned approximately parallel. The telescopes utilized RCA 7151 Q photomultipliers with S20 photocathodes as the sensors. The instrument was designed to yield trajectory information for those particles with a good signal-to-noise ratio.

A low signal-to-noise ratio in most of the events observed made the orbit analysis a far more difficult process than was originally envisioned. In general, the results achieved with this sensor were of limited value.

The Infrared Astronomical Satellite (IRAS) contains an orbital sensor designed for astronomical observations. It consists of a telescope which surveys the sky such that during each sun synchronous polar orbit a 360° ring of width equal to the focal plane array cross scan field of view is swept. The 1° per day orbital precession sweeps successive rings.

The detector array consists of detectors for bands of 8-15 microns, 15-30 microns, 30-50 microns, and 50-120 microns. A 60 cm aperture telescope cooled to a 4°K temperature is used to focus a 1° field of view onto the detectors which lie in the focal plane.

Each detector has an auxiliary lens so that the entire entrance aperture is focused onto each array element. The detector performance is noise limited by the zodiacal background rather than by detector technology or the telescope itself.

To evaluate the detectability of small particles using a passive infrared sensor such as IRAS requires that the self-radiation from the particle be known. Assuming grey body radiation and an isotropic radiator, the radiated power per micron is given by

$$P = A \int \epsilon_{\lambda} W_{\lambda} d\lambda \quad (3.2-1)$$

where A is the particle surface area, ϵ_{λ} is the particle emissivity as a function of wavelength, and W_{λ} is Planck's black body radiation function corresponding to the particle temperature.

The actual particle temperature is determined by the balance between the thermal input from the sun and the radiated energy. This depends upon the absorption at wavelengths near the solar peak and the emissivity in the infrared. It can be a strong function of the particle material.

Table 3.2-1 gives the values of W_{λ} for various particle temperatures and wavelengths. The radiation flux at the IRAS detector array depends upon the particle radiated-power density, the range of the particle, the telescope aperture, the telescope efficiency, the particle angular rate, and the detector performance or noise equivalent flux density. The detector parameters for the IRAS system are given in Table 3.2-2 [Aumann and Walker, 1977].

TABLE 3.2-1. BLACKBODY RADIATION, WATTS/CM²/MICRON

Wavelength	Temperature, °K				
	300	250	200	150	100
10μ	3.12x10 ⁻³	1.19x10 ⁻³	2.8 x10 ⁻⁴	2.25x10 ⁻⁵	2.1 x10 ⁻⁷
20μ	1.17x10 ⁻³	6.98x10 ⁻⁴	3.3 x10 ⁻⁴	9.76x10 ⁻⁵	8.8 x10 ⁻⁶
60μ	3.74x10 ⁻⁵	3.0 x10 ⁻⁵	2.1 x10 ⁻⁵	1.22x10 ⁻⁶	4.8 x10 ⁻⁶
100μ	6.1 x10 ⁻⁶	4.8 x10 ⁻⁶	3.55x10 ⁻⁶	2.33x10 ⁻⁶	1.16x10 ⁻⁶

TABLE 3.2-2. IRAS DETECTOR PARAMETERS

Wavelength Band	Detector Type	Detector Bandwidth	Quantum Efficiency	Zodiacalcal NEP	NEFD Watts/cm ²
8-15μ	Si:As	4 Hz	.3	1.4x10 ⁻¹⁶	2.4x10 ⁻¹⁹
15-30μ	Si:Sb	4 Hz	.3	.9x10 ⁻¹⁶	1.6x10 ⁻¹⁹
30-50μ	Ge:Be	2 Hz	.2	.7x10 ⁻¹⁶	.8x10 ⁻¹⁹
50-120μ	Ge:Ga	1 Hz	.1	.7x10 ⁻¹⁶	.6x10 ⁻¹⁹

Using the listed NEFD values, the signal to noise ratio at the detector is

$$S/N = \frac{A \int \epsilon_{\lambda} N_{\lambda} d\lambda}{4\pi R^2 \text{NEFD}} \left[\frac{R\Omega}{v_t} \right] \quad (3.2-2)$$

where R is the range to the particle, Ω is the sensor scanning rate, v_t is the particle linear velocity perpendicular to the observation directions, and NEFD is the detector sensitivity.

The term in the brackets is a factor to compensate for the reduced detectability of objects moving faster than the telescope scanning rate. This assumes that the telescope detection bandwidths are matched to the angular scanning rate.

For a stationary object, the term in brackets is neglected. It has been stated that in the 8-15 μ band, the IRAS telescope could detect a 300°K object of 3 cm radius at a range of 3000 km with a 10 db signal-to-noise ratio. To verify this, Equation 3.2-2 will be used to estimate the S/N for such an object.

From Table 3.2-1, we see that at 10 μ the radiation from a 300°K blackbody is 3.2×10^{-3} watts/cm²/micron. The total radiated power becomes $28\pi a^2 \times 3.12 \times 10^{-3} = 2.46$ watts for a 3 cm radius object. At a range of 3000 km, the power density is 2.18×10^{-18} watts/cm². The NEFD for band one is 2.4×10^{-19} watts/cm², giving an S/N of 9.5 db, very close to the 10 db quoted.

To estimate the detectability of moving particles of various sizes, Equation 3.2-2 indicates that the detection range is proportional to the emissivity, the black body radiances, and the square of the particle radius, i.e.

$$R_{\text{Det}} = K a^2 \epsilon \int W_{\lambda} d\lambda \quad (3.2-3)$$

where K is a constant containing the detector parameters and the particle velocity.

Table 3.2-3 lists the detection ranges for 300°K particles in band 1 assuming an emissivity of .5 and a 10 db signal-to-noise ratio.

TABLE 3.2-3. IRAS DETECTION RANGES

Particle Size (cm)	Stationary Particle Detection Range (km)	7 km/sec Moving Particle Detection Range (km)
5	3500	3500
1	700	700
.5	350	350
.1	70	43

It should be noted that the detection ranges listed in Table 3.2-3 for a 1 mm moving particle assumes that the response of the IRAS detectors degrades linearly with the ratio of the maximum possible observation time corresponding to the angular rate of the particle with the detector response time determined by the reciprocal of the bandwidth of the system electronics. This may, in fact, not be the case and the degradation could be much more severe. To determine the true response of the IRAS instrument to rapidly moving particles requires more knowledge about the details of the instrument than were available at the time of this study.

3.3 EVALUATION OF OPTIONS

ORIGINAL PAGE IS
OF POOR QUALITY

3.3.1 Orbiting Radar Sensor

To estimate the potential detection performance of an orbital radar sensor free of preconceived concepts about the sensor configuration, we can start with the radar equation, 3.1-3. It will be instructive to write this equation in a form which exhibits the true constraints on the radar system. These include the maximum available transmitter power output, the physical size of the antenna, and the maximum available integration time.

The most efficient radar is one in which only coherent integration is used. For such a radar, the radar equation can be written as

$$S/N = \left[\frac{P_t A^2 \sigma \tau}{\lambda^2 R^4} \right] \left[\frac{L}{4\pi k T_e} \right] \quad (3.3-1)$$

In this expression, the second term in the brackets depends upon good design practice and component state of the art and cannot be varied to any significant extent; the parameters appearing in this term were defined in Eq. 3.1-3.

The first expression is different than before and includes A , the antenna area, and a factor τ , the coherent integration time. This factor is approximately the reciprocal of the system effective coherent bandwidth B_e used in the previous equation.

From the first factor, the relationship between the system parameters and the signal-to-noise ratio is apparent. The operating wavelength and the antenna area appear to the second power; if possible, improvements in these areas would be of particular benefit.

Unfortunately, there are limits to the antenna size that can be used. Also, at the present time and in the near future, the radar wavelength is constrained to those for which space qualified transmitter power amplifiers exist. These were discussed in Section 3.2.1.

The particle cross section also depends upon the radar wavelength; however, in general it is not under the designer's control. Similarly, the available transmitter power output is limited by the availability of space qualified power amplifier tubes.

This leaves only the detection range, and the integration time as variables potentially adjustable by the system design and operational approach.

To define the integration time, the antenna beamwidth, the total angular coverage, and the scanning logic must be determined. The options range from a relatively wide beamwidth staring system to a narrow pencil beam which is scanned sufficiently rapidly that the scan repetition period is less than the transit time of a debris particle through the coverage volume.

If the angular coverage is Ω steradians, and the antenna beamwidth is θ_{HP}^2 , the number of antenna beam positions required to cover an angular area is Ω/θ_{HP}^2 . If the particle transit time through the coverage volume is T_p , then the maximum integration time becomes $\tau = T_p/N = T_p \theta_{HP}^2/\Omega$.

The first factor in the signal-to-noise expression then becomes

$$\left[\frac{P_t A^2 \sigma T_p \theta_{HP}^2}{\lambda^2 \Omega R^4} \right] \quad (3.3-2)$$

To examine the available radar sensor options in more detail requires that the particle transit time and the angular coverage be defined. These are obviously inter-related.

The coverage volume required can be estimated in several ways. The optimum would be to determine the particle flux sampling rate required to estimate the flux density in a statistically meaningful manner. Another way, which interacts significantly with the radar sensor, is to sample a large enough volume to insure a high enough detection rate that sensor false alarms due to noise do not present a problem.

For example, Tables 3.3-1 and 3.3-2 give the detection ranges required to provide a detection rate of one debris particle per day for the case of a sensor looking along the spacecraft velocity vector with a 60 degree field of view and one looking perpendicular to the velocity vector with a 4 degree field of view.

This data indicates that at the lower altitudes, detection ranges considerably larger than 10 km would be required to provide detection rates as high as one per day.

TABLE 3.3-1. DETECTION RANGE (KM) REQUIRED FOR ONE DETECTION EVENT PER DAY--CONE ANGLE = 60°--CONE ORIENTED WITH AXIS POINTING ALONG THE FLUX VECTOR

h	R _{cons} ¹⁰	R _{cons} ²⁰	R _{1cm} ¹⁹⁹⁵	R _{1mm} ¹⁹⁹⁵
275	68.9	57.6	37.5	24.9
400	32.9	28.6	13.9	6.8
500	19.7	16.1	6.0	2.7
600	18.2	14.5	4.5	0.83
700	16.1	11.2	3.0	0.25
800	15.2	13.9	3.0	0.38
1000	18.2	14.9	3.0	0.25

TABLE 3.3-2. DETECTION RANGE (KM) REQUIRED FOR ONE DETECTION
EVENT PER DAY--CONE ANGLE = 4°--CONE ORIENTED
WITH AXIS POINTING IN RADIAL DIRECTION

h	R _{cons} ¹⁰	R _{cons} ²⁰	R _{1cm} ¹⁹⁹⁵	R _{1mm} ¹⁹⁹⁵
275	342	288	189	124
400	164	141	69.9	33.8
500	98.0	80.0	29.9	13.4
600	90.9	73.3	22.1	4.2
700	80.0	56.2	15.0	3.1
800	76.0	69.9	15.0	1.9
1000	90.2	74.4	15.0	1.3

The average transit time of a particle crossing a sensor field of view perpendicular to the axis is given by

$$T_p = \frac{\pi R \sin\sqrt{\Omega}}{4 v_t} \quad (3.3-3)$$

where Ω is the effective sensor angular coverage area. Using this in Eq. 3.3-2 gives

$$\frac{\pi P_t A^2 \sigma \sin\sqrt{\Omega} \theta_{HP}^2}{4 \lambda^2 \Omega R^3 v_t} \quad (3.3-4)$$

The half-power beamwidth of an antenna is related to the antenna area by approximately

$$\theta_{HP}^2 = \frac{\lambda^2}{A} \quad (3.3-5)$$

The exact relationship depends upon the aperture illumination function; however, it is typically within 50 percent of the above value. Using this, expression 3.3-4 becomes

$$\left[\frac{\pi P_t \lambda^2 \sigma \sin \sqrt{\Omega}}{4 \Omega \theta_{HP}^2 R^3 v_t} \right] \quad (3.3-6)$$

To reduce this further requires that the system be identified as either a scanning system or a staring system. For a scanning system expression 3.3-6 is the reduced expression.

For a staring system where $\Omega = \theta_{HP}^2$, this term becomes

$$\left[\frac{\pi P_t \lambda^2 \sigma \sin \theta_{HP}}{4 \theta_{HP}^4 R^3 v_t} \right] \quad (3.3-7)$$

and if Ω is small enough that $\sin \sqrt{\Omega} = \sqrt{\Omega}$, expression 3.3-7 becomes

$$\left[\frac{\pi P_t \lambda^2 \sigma}{4 R^3 \theta_{HP}^3 v_t} \right] \quad (3.3-8)$$

The total signal to noise ratio becomes

$$S/N = \left[\frac{\pi P_t \lambda^2 \sigma}{4 R^3 \theta_{HP}^3 v_t} \right] \left[\frac{L}{4 \pi k T_e} \right] \quad (3.3-9)$$

For a system using a conical antenna beam covering a conical area, the signal-to-noise ratio for a staring sensor versus the signal-to-noise ratio for the same sensor using a scanning format becomes from expressions 3.3-6 and 3.3-9.

$$\frac{S/N \text{ (staring)}}{S/N \text{ (scanning)}} = \frac{\Omega \sin\theta_{HP}}{\theta_{HP}^2 \sin\Omega} \quad (3.3-10)$$

This indicates a signal-to-noise advantage for a staring sensor. This analysis pertains only to a system using conical beams, a conical coverage zone, and monitoring particles which are crossing perpendicular to the beam look-direction such as a system looking radially upward at particles in circular orbits.

This advantage is due to the increased integration time available to the staring sensor and applies only to detection. The tracking ability of such a sensor has not been considered.

If a radar sensor is configured to look forward with a staring conical beam, the average transit time for this case conservatively becomes

$$\frac{R}{2v_t} \cos\left(\frac{\theta_{HP}}{2}\right) \quad (3.3-11)$$

where R is the range to the particle. In this case this is also the average available integration time. The initial factor in the signal-to-noise ratio now becomes

$$\frac{P_t \lambda^2 \sigma \cos\left(\frac{\theta_{HP}}{2}\right)}{2 R^3 \theta_{HP}^4 v} \quad (3.3-12)$$

This can be compared with the same system staring upward as given by expression 3.3-7 to give

$$\frac{S/N(\text{Forward})}{S/N(\text{Upward})} = \frac{2 \cos\left(\frac{\theta_{HP}}{2}\right)}{\pi \sin \theta_{HP}} \quad (3.3-13)$$

This indicates that a forward staring system with a one radian coverage has no significant advantage over the same system staring upward in particle detectability. A definite advantage exists, however, for narrower beamwidths.

Typical numbers to illustrate potential detection ranges will be used. These are: a frequency of 15 GHz corresponding to the SEASAT altimeter, a 2 kw peak power output, a 500°K effective receiver noise temperature, an antenna efficiency of .6, a system loss of 4.7 db, a required signal-to-noise ratio of 13.2 db, and a particle velocity of 7 km/sec. With these parameters and Equation 3.3-6 for an upward scanning system, the detection range becomes

$$R_{\text{scan}}^u = 3.78 \times 10^4 \left[\frac{\sigma \sin \sqrt{\Omega}}{\Omega \theta_{HP}^2} \right]^{1/3} \quad (3.3-14)$$

For an upward staring system, the detection range becomes

$$R_{\text{stare}}^u = 3.78 \times 10^4 \left[\frac{\sigma \sin \theta_{HP}}{\theta_{HP}^4} \right]^{1/3} \quad (3.3-15)$$

For a forward staring system, the detection range becomes

$$R_{\text{stare}}^F = 3.24 \times 10^4 \left[\frac{\sigma \cos\left(\frac{\theta_{\text{HP}}}{2}\right)}{\theta_{\text{HP}}^4} \right]^{1/3} \quad (3.3-16)$$

A similar analysis can be applied to a system using a non-circular antenna beam. For example, if the half-power beamwidths in the two principle planes are designated θ_1 , θ_2 , then the signal-to-noise ratio expression for a vertically oriented fan beam radar system becomes

$$S/N = \left[\frac{P_t \lambda^2 \sigma}{\theta_1 \theta_2^2 R^3 v_t} \right] \left[\frac{L}{4\pi k T_e} \right] \quad (3.3-17)$$

with θ_1 the beamwidth parallel to the spacecraft velocity vector and θ_2 the beamwidth perpendicular to the velocity vector.

The signal-to-noise ratio given in Eq. 3.3-17 is for a true fan beam where $\theta_2 \gg \theta_1$. For a narrow conical beam system of beamwidth θ_1 , which is scanned over a coverage zone θ_2 , the signal-to-noise ratio is reduced by the ratio of θ_2/θ_1 .

Using the same parameters as previously, the detection range for this type of system becomes

$$R_{\text{fan}}^U = 4.08 \times 10^4 \left[\frac{\sigma}{\theta_1 \theta_2^2} \right]^{1/3} \quad (3.3-18)$$

The detection ranges on small particles are generally quite small for all of these systems. For example, for the system of Table 3.3-1, the detection range becomes

$$R = 2.9 \times 10^4 \sqrt[3]{\sigma} \quad (3.3-19)$$

and for a 4 mm particle with a radar cross section of 1.76×10^{-5} at 15 GHz the detection range is 755 m.

For the system of Table 3.3-2, looking upward, the detection range becomes

$$R = 4.6 \times 10^6 \sqrt[3]{\sigma} \quad (3.3-20)$$

and for a 4 mm particle the detection range becomes 12 km.

The detection ranges for 1 mm, 5 mm, and 1 cm particles for the various systems are given in Table 3.3-3 for various coverage and beamwidth options.

The detection ranges presented in Table 3.3-3 are very small for a 1 mm particle except for the very narrow-beam forward-staring system. In general, there are no simple ways to improve these. Significantly higher power output transmitters are generally not available for space applications. Going to a higher frequency than 15 GHz would at best give a performance comparable to the 5 mm and 1 cm particles which are out of the Rayleigh scattering region and exhibit a projected area dependence of the cross section.

One method that could potentially have application to a forward looking radar sensor would be to use a sequential detection algorithm which would result in a high cumulative detection probability even through the single look probability is well below the 90 percent assumed in the calculations for Table 3.3-3. This would not represent a near term solution, however.

TABLE 3.3-3. RADAR DETECTION RANGES

Coverage Cone	1 mm Diameter					
	Starting Upward Circular	Starting Forward	Starting Upward 1° Fan Beam	Upward Scanning 1° Fan Beam	Starting Upward 5° Fan Beam	Upward Scanning 5° Fan Beam
60°	0.06 km	.05 km	.25 km	.06 km	.145 km	.06 km
30°	0.12 km	.12 km	.39 km	.12 km	.23 km	.13 km
10°	0.35 km	.59 km	.818 km	.38 km	.48 km	.38 km
5°	0.70 km	1.4 km	1.3 km	.76 km	.70 km	.70 km
1°	3.6 km	11.6 km	3.8 km	3.8 km		

Coverage Cone	5 mm Diameter					
	Starting Upward Circular	Starting Forward	Starting Upward 1° Fan Beam	Upward Scanning 1° Fan Beam	Starting Upward 5° Fan Beam	Upward Scanning 5° Fan Beam
60°	1.4 km	1.2 km	6.2 km	1.58 km	3.6 km	1.6 km
30°	2.9 km	3.1 km	9.8 km	3.2 km	5.7 km	3.1 km
10°	8.8 km	13.5 km	20.5 km	9.5 km	12.0 km	9.5 km
5°	17.6 km	34.0 km	32.5 km	19.0 km	17.6 km	17.6 km
1°	88.0 km	290 km	88.0 km	88.0 km		

Coverage Cone	1 cm Diameter					
	Starting Upward Circular	Starting Forward	Starting Upward 1° Fan Beam	Upward Scanning 1° Fan Beam	Starting Upward 5° Fan Beam	Upward Scanning 5° Fan Beam
60°	1.45 km	1.2 km	6.5 km	1.66 km	3.8 km	1.7 km
30°	3.0 km	3.3 km	10.4 km	3.3 km	6.6 km	3.6 km
10°	9.3 km	14.2 km	21.6 km	10.0 km	12.6 km	10.0 km
5°	16.5 km	35.8 km	34.2 km	20.0 km	18.5 km	18.5 km
1°	92.7 km	306 km	92.7 km	92.7 km		

In general, the data indicates that if a large coverage angle is desired, then a simple upward staring fan beam is the best solution.

In the preceding discussion, some analysis of the options open to a radar sensor designer has been presented. Since a debris particle must be detected prior to being tracked, detection performance was the major consideration.

In comparing the relative merits of a sensor configuration, whether various radar configurations such as listed in Table 3.3-3 or comparing sensor types such as radar and electro-optical, it is necessary that the value of the sensor relative to the accomplishment of a specific objective be known, and that sensors of equal value be utilized when costs, weights, power requirements, etc. are compared.

At the present time it is difficult to assess the relative value of sensors with widely varying collection areas, detection ranges for a given particle size, complexities, costs, weight, and power requirements, and useful lifetimes.

4.0 MICROPARTICLE DETECTOR SYSTEMS

4.1 IMPACT SENSORS

Various types of impact sensors have been developed for detecting micrometeoroids and have been effectively used in space experiments. A comprehensive discussion of several of these techniques has been presented in the text "Space Physics" [KeGalley and Rosen, 1964].

4.1.1 Microphone Sensors

Microphone or acoustical impact detectors are responsible for a large percentage of all the data on micrometeoroids obtained in space experiments. The sensor consists of a piezoelectric crystal which is attached to a metal surface that acts as a sounding board. When a micrometeoroid strikes the metal plate, an electrical signal is generated, and the amplitude of the signal is some function of the velocity and mass of the particle. A typical sensitive area is approximately 10^{-2} meter².

Several disadvantages of this detection method include the following:

- The sensitivity varies over the surface of the sounding board. It is a function of distance of the point of impact to the point of an angular dependence around the point of support.
- The response of the detector may be considerably different for the mass and velocity range that is used for calibration compared with the actual ranges of these variables which are found to exist in space.

- The average velocity is unknown. This point is usually dismissed by a statement that when the correct average velocity is known the data may easily be corrected. However, this may be a questionable procedure, since there may be wide variations in the velocity of the micrometeoroids.

The sensitivities that have been used in space experiments so far have ranged in value to as low as 10^{-8} kg-meter/sec. In laboratory experiments, using micron-sized iron spheres (mass about 10^{-14} kg) accelerated to speeds of 8 km/sec, responses have been obtained from a lead-zirconate crystal [Friichtericht, 1964]. The crystal was packaged and suspended from a rubber grommet with its axis parallel to the beam of particles from an accelerator.

4.1.2 Impact Light Flash Sensors

Some of the energy that a high-speed particle transfers to a surface upon impact results in light emission. The intensity of radiation depends on the energy of the projectile. In spite of the very limited information on the performance of light-flash detectors, they have been used on several space experiments [Berg, 1956, Aerospace Year Book, 1969]. The experimental arrangement was a photomultiplier with a thin layer of aluminum (about 1 to 2000 Å thick) evaporated onto the face to shield the tube from the background radiation. The lower limit of mass sensitivity to hypervelocity particles of such a detector is in the range of 10^{-10} kg. Therefore, such a sensor can play a role in answering questions relating to the lower limit of masses of micro-meteoroids.

4.1.3 Impact Ionization Sensors

A phenomenon that is related to the impact light flash is impact ionization. There is sufficient energy per atom at

hypervelocities to reach the ionization potentials of most materials. Although it is not clear what the ionization probabilities are, it is probable that the cross sections for such processes increase with velocity.

In situ detectors based on the measurement of impact ionization have been flown on several space missions (Pioneer 8/9, HEOS-2, and Helios 1/2). Currently two flights are being prepared for Galileo and ISP missions.

The mission of Pegasus, the Meteoroid Technology Satellite, was to define the magnitude and direction of medium-size meteoroids in the near-earth space environment [Aerospace Year Book, 1969]. Three Pegasus spacecraft were sent into varying orbits, 300 to 500 miles high, transmitting meteoroid detection information on a daily basis. The spacecraft used a deployed wing 96 feet long and 14 feet high. Its capacitor detectors of varying thickness provided over 2,000 square feet of area designed to count meteoroid hits for at least 1 year in space. Three spacecraft, launched in 1965, were still operational and returning useful data in 1968, at which time they were turned off.

4.1.4 Penetration Sensors

One type of detectors use the penetration of a thin wall to obtain a detectable effect. Three types of penetration detectors are pressurized cells, steel-covered grids, and copper-wire cards.

The pressurized cells consist of an enclosed chamber filled with some gas such as helium. A micrometeoroid penetrating the wall of the chamber leads to the subsequent leakage of gas and the pressure loss leads to the actuation of a switch. The sensor has then completed its mission, since it is no longer sensitive. In order to be useful, it is necessary to employ a large number of them on a given experiment; 160 sensors were

carried on Explorer 16. Three thicknesses of wall were chosen, and each sensor had an area of about $1/10 \text{ ft}^2$. Explorer 23 used single walls of stainless steel with $25 \text{ }\mu\text{m}$ and $50 \text{ }\mu\text{m}$ thicknesses.

Explorer 46 also used pressurized cells for the dedicated study of meteoroids and meteoroid protection. The spacecraft consisted of four deployable wings which were the target panels [Humes, 1981]. Each wing consisted of three flat panels containing eight pressurized cells. The pressurized cells were long, narrow cells running the length of the panel.

During launch, the panels were rolled up like window shades and the cells were not inflated. After the spacecraft was injected into Earth orbit, booms were used to unroll the wings, then the cells were pressurized.

It was intended that all four wings would extend to a length of 3.20 m, but a malfunction in the deployment apparatus left two opposing wings only partially deployed. It has been estimated, from the time the boom drive motor operated, that the partially deployed wings were extended to a length of 1.6 m. This malfunction created an unfavorable spacecraft inertia ratio and caused a transfer from the preferred spin stabilization mode to a rotational motion which invalidated the passive thermal design concept. As a result, the prime telemetry system and its battery power supply were left in constant sunlight. The consequent overheating resulted in a command anomaly and a decision to discontinue interrogation of the prime telemetry system. The data for the small-meteoroid population experiment were transmitted only through the prime telemetry system and were lost when that system was not interrogated.

The unfavorable orientation of the spacecraft also left the meteoroid velocity detectors in sunlight which caused the front stations to develop a permanent electrical short.

The data from the meteoroid bumper experiment were transmitted through a backup telemetry system which operated

continuously when the spacecraft was in sunlight, so that no data were lost because of the malfunction.

The essential data obtained from the bumper experiment were the times at which each cell was penetrated by a meteoroid. Those penetrations were detected by observing the loss in pressure that accompanied the penetration.

The concentration of meteoroids in interplanetary space between 1.0 and 5.1 AU and near Jupiter was measured with pressurized cell penetration detectors on Pioneer 10 [Humes et al, 1974]. These detectors have a sensitivity of approximately 2×10^{-9} g.

The meteoroid detection instrument on the Pioneer 10 spacecraft consisted of 234 cells pressurized with a gas mixture and a device to monitor the pressure in each cell. The cell walls were 25- μ m-thick stainless steel. When a meteoroid penetrates the wall, the gas escapes from the cell, and the loss of pressure is detected.

The detectors were fabricated in 13 panels, each having 18 cells.

The experiment was fabricated as two essentially independent instruments to increase reliability. One instrument consists of six panels. The other instrument consists of seven panels and the associated electronics. A common dc/dc power converter supplies power for both channels.

On Explorer 16 a grid consisting of a thin layer of gold deposited on a thin Mylar layer was used. The projected area of a given sensor was about 0.1 ft².

Another closely related sensor is the copper-wire card detector, which consists of a continuous winding of copper wire on an insulating base. In this case the wire thickness determines the layer that has to be penetrated for a count to occur. When a particle breaks one of the wires, the resistance of the winding changes and a count may be detected. On Explorer 16, copper wires of 2 and 3 mils were used and the sensitive area of each detector was about 1/20 ft².

The difficulties associated with pressurized cells also applies to the covered grids and copper-wire detectors, which are one-count-only devices. Their calibrations are not determined by direct experiment but involve crude theoretical estimates.

Another type of puncture detector is one in which a puncture leads to a change of some property but does not ruin the counter. However, the effect of the puncture remains; that is, there is no healing process. An example is the cadmium-sulfide cell system. The material to be penetrated is a thin layer of Mylar (1/4 mil) with a thin alyer of aluminum (about 10^3 \AA) deposited on one or both sides of the Mylar. The Mylar is mounted to prevent light reaching the CdS cell except through any punctures that may occur in the Mylar. As penetrations occur, the output of the cell changes. In principle, the size of a given increment of the cell output may be related to the size of the hole created by the micrometeoroid penetration.

Some work has been done on calibrating this detector. The STL microparticle accelerator has been used, and some preliminary data on the relation of hole size to particle size have been found. Detectors of this type have already been used on space experiments (Explorers 7 and 16). The exposed area per cell is about 4 to 5 in².

Another type of penetration detector is still of the puncture variety but has an additional important feature; the effect of a puncture on the output effectively disappears after a given count and the system is ready for a second puncture. Various systems have been tried, but the basic principle is that of a parallel plate condenser. In one variety, a thin layer of Mylar (1/4 mil) with aluminum deposited on each side acts as the condenser. A small voltage is then applied between the aluminum "plates." When a particle penetrates the detector, the condenser discharges through the ionized region in the Mylar. The break then appears to heal, the condenser recharges, and the system is ready for a second count. Another combination consists of a

layer of MgO about 1000 Å thick with aluminum deposited on each side. The system seems to heal itself.

This general type of detector will, undoubtedly, prove more and more useful in the micrometeoroid field. (Again, the main difficulty is the correct determination of the minimum velocity and mass required for a penetration.) A further point to study is the nature of the healing process itself. For example, is there a difference between small and large particles, that is, those that are less than or greater than the condenser thickness?

4.1.5 Multiparameter Detectors

It is essential that a multiparameter type of detector be used if both mass and velocity are to be obtained. Some efforts have already been made in this direction. An example is a two-parameter system for time-of-flight techniques.

This system uses the condenser-type detector to provide the marker pulses for the flight-time measurement. Two very thin MgO (1500 Å) condensers are separated by about 10 cm, so that the flight times are about 10 μsec. After passing through the two-marker pulse detectors, the particle then impacts any detector for which the response as a function of mass and velocity is known. This last detector must have a response time comparable to the flight times measured. This last criterion essentially rules out microphones; however, light-flash and ionization detectors may be used.

There are some difficulties with this arrangement. First, the energy loss in the condensers will lead to an error in the velocity. Second, the passage of micrometeoroids through thin foils often leads to fragmentation. Studies of energy loss and other phenomena involved in the passage of micrometeoroids through thin foils should be pursued to clarify these points. However, this system shows real promise of leading to a multiparameter detector.

The system may be modified by eliminating the second marker detector. If the rise time of the output of the mv detector is short enough, the rising portion of this pulse may be used for the time-of-flight part of the measurement. The elimination of the second penetration layer of condenser material would obviously be helpful.

The next step would be to use a single impact surface and measure at least two phenomena that result from a given impact. An example of this technique is the system that was placed aboard Ranger 1 [Alexander, 1961]. The impact surface was the face of a photomultiplier tube, and a microphone was attached to the glass envelope of the tube. This system, then, was a light-flash-acoustical detector.

In detectors of this type there are two thresholds. Therefore, three types of data are presented: pulses from the acoustical sensor, pulses from the light-flash sensor, and coincident pulses from the two sensors. A combination of a few experimental results and extrapolation from hypervelocity data and crude theory was made to interpret the data from the two-parameter detector on the Ranger 1.

Of course, there are other combinations of effects that may be used. For example, the ionization effect may be combined with the acoustical effect. Since the light flash and ionization effect probably have the same velocity-dependence, their combination may not be a useful one. However, as more details are learned of these phenomena and other new impact effects, it is clear that the multiparameter detectors will be the systems to use for experimentation.

5.0 EVALUATION OF THE "PIGGY-BACK" OPTION

A generalized concept of piggy-backing will be discussed in this section. Piggy-backing will be understood as sharing the resources of another program to reduce the cost of acquiring debris data. The sharing might consist of sharing the ride on a free-flyer, making use of data acquired for other purposes, or acquiring data from orbital systems not designed to provide debris data. Based on the factors considered in this section, there would, for example, appear to be many Shuttle flights in the current manifest which offer the possibility for obtaining debris data through various forms of piggy-backing. These opportunities are summarized in Table 5.0-1, and discussed further in the following subsections.

5.1 SHARING THE RIDE ON FREE-FLYERS

The option for "piggy-backing" a debris detection system onto an existing spacecraft offers an alternative for getting detectors into space at considerably less cost than required to prepare a free-flyer. Such an arrangement allows a detector to be flown without requiring it to supply its own power, attitude control, or telemetry, but it does so while imposing perhaps unacceptably severe constraints on the detector configuration and mode of operation and on the region of space the detector will be able to scan.

The Search and Rescue (SAR) module being carried on the TIROS-N/NOAA satellite is an example of a successful piggy-back operation. The spacecraft was designed and built by NASA for the National Oceanic and Atmospheric Administration (NOAA). The SAR module was also originally conceived as a free-flyer, but cost restrictions forced the alternative approach of piggy-backing to be taken. The SAR subsystem has become a permanent part of the NOAA satellite, with plans to remain on it at least until the

TABLE 5.0-1. A SUMMARY OF PIGGY-BACKING OPPORTUNITIES ON FLIGHTS APPEARING IN THE CURRENT SHUTTLE MANIFEST

SCHEDULED LAUNCH DATE	SHUTTLE FLIGHT NUMBERS	DEPLOYABLE LEO SATELLITES	DOE DEDICATED FLIGHTS	SHARED DOE FLIGHTS	NASA-SPONSORED ATTACHED PAYLOADS	NON-NASA SPONSORED ATTACHED PAYLOADS	OPPORTUNITY PAYLOADS	SPACELAB FLIGHTS	SPACE TELESCOPE	EDWE	RETRIEVAL FLIGHTS	SUMMARY
03/00/83	6											
05/00/83	7											
07/00/83	8											
09/30/83	9											
11/03/83	10											
01/29/84	11											
03/18/84	12											
04/13/84	13											
05/18/84	14											
06/04/84	15											
07/01/84	16											
07/28/84	17											
08/23/84	18											
09/15/84	19											
10/11/84	20											
11/03/84	21											
12/04/84	22											
01/05/85	23											
01/30/85	24											
02/26/85	25											
04/18/85	26											
05/14/85	27											
06/11/85	28											
07/09/85	29											
08/03/85	30											
09/01/85	31											
09/28/85	32											
10/15/85	33											
10/24/85	34											
11/22/85	35											
12/17/85	36											
02/08/86	37											
02/19/86	38											
03/01/86	39											
03/25/86	40											
05/30/86	41											
07/02/86	42											
07/10/86	43											
08/01/86	44											
08/12/86	45											
09/21/86	46											
09/27/86	47											
10/04/86	48											

ORIGINAL PAGE IS OF POOR QUALITY

SCHEDULED LAUNCH DATE	SHUTTLE FLIGHT NUMBERS	DEPLOYABLE LEO SATELLITES	DOE DEDICATED FLIGHTS	SHARED DOE FLIGHTS	NASA-SPONSORED ATTACHED PAYLOADS	NON-NASA SPONSORED ATTACHED PAYLOADS	OPPORTUNITY PAYLOADS	SPACELAB FLIGHTS	SPACE TELESCOPE	EDWE	RETRIEVAL FLIGHTS	SUMMARY
11/07/86	47											
11/20/86	48											
12/04/86	49											
01/02/87	50											
01/09/87	51											
01/21/87	52											
02/10/87	53											
03/04/87	54											
03/23/87	55											
04/11/87	56											
05/01/87	57											
05/19/87	58											
06/06/87	59											
06/15/87	60											
06/27/87	61											
07/24/87	62											
08/04/87	63											
09/20/87	64											
09/30/87	65											

Δ = Reflight Opportunities

next generation of Shuttle-compatible NOAA satellites are introduced in the 1988-1990 time frame. Figure 5.1-1 shows the TIROS-N spacecraft.

The NOAA satellite, which flies on the Atlas/F, was designed and built with a 25 percent weight, power, and volume margin. Experiments requiring one or two flights can draw on these margins without impacting the overall spacecraft configuration, giving the NOAA satellite considerable flexibility in accommodating new experiments at minimal cost. However, since the SAR module was to become a permanent part of the NOAA satellite, the SAR program was required to pay for the redesign required to maintain the weight, power, and volume margins. In the reconfiguration of the TIROS-N, 18" was added to the length and a higher capacity power system was introduced.

The redesign and testing of the modified TIROS-N was done at no cost to NOAA. The cost to the SAR project was \$14.6 million, of which \$9.4 million was for system design and \$4.8 million was for testing. This cost compares to \$100 million cost for design and construction of the TIROS-N and \$22 million for a single launch of the Delta launch vehicle. Development time for the SAR was also short - 3 years from decision to piggy-back to first flight.

Based on the likely future carrier traffic, two types of Debris Detection and Monitoring (DDM) piggy-back modules might be considered. A "smart" design would require attitude control, power, telemetry downlink, and perhaps an accurate spacecraft ephemeris; such a module might contain remote sensor detectors for large particles or microparticle detectors. Candidate carriers for this type of module would be any of the LEO satellites. A "dumb" DDM module would ride on a retrievable carrier, getting its data to the researcher after retrieval had been accomplished. While it could be designed with varying degrees of sophistication, a large-area impact counter requiring only

ORIGINAL PAGE IS
OF POOR QUALITY

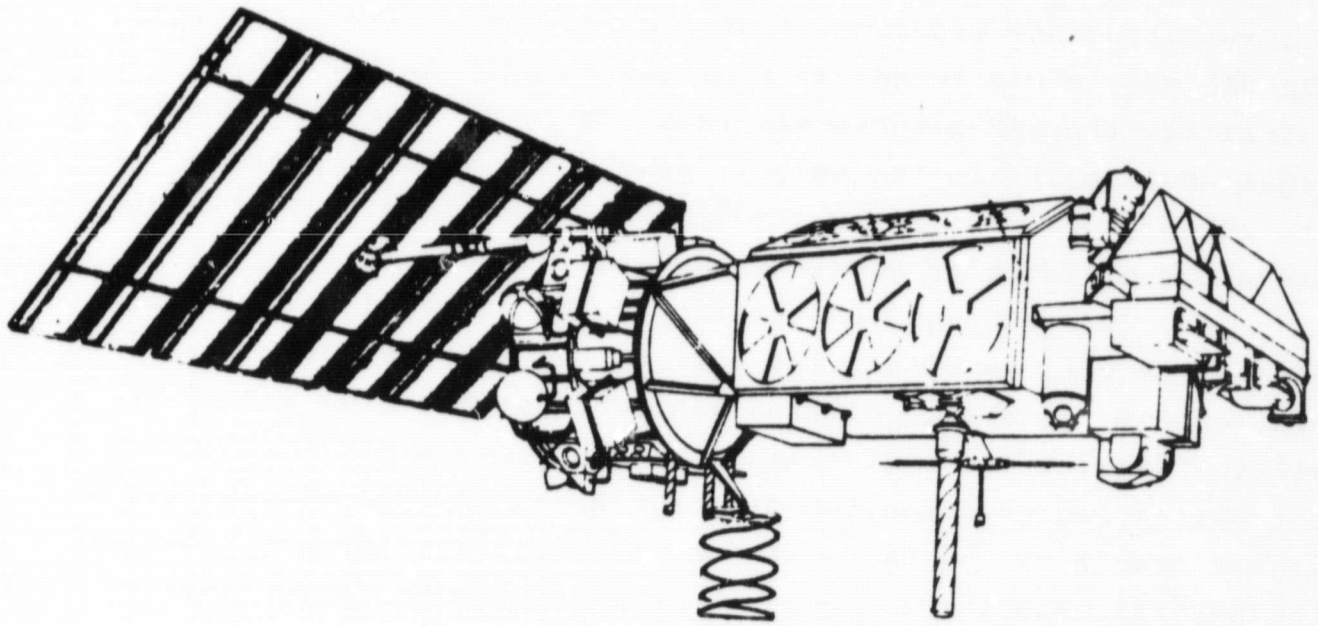


FIGURE 5.1-1. DRAWING OF THE TIROS-N SATELLITE

attitude control would be an example of a dumb module. Candidate carriers would be LDEF, LEASAT, and Eureka.

A smart DDM module would have several factors working in its favor. Presumably it could in fact might prefer to look in the direction of the velocity vector or away from the Earth's surface, while most instrumentation in LEO looks at the Earth. This reduces the likelihood that the detection instrumentation will affect the other instruments on board the spacecraft and, in fact, the electronics interference produced by the complex instrumentation such as a phased array radar might be the most difficult barrier to overcome.

Candidate carriers for the DDM would come from NASA, DoD, and the outside user community, the last of which includes commercial US, non-NASA/non-DoD government U.S., and foreign programs.

Battelle has been tasked by NASA Headquarters to generate the NASA outside user payload model, an assessment of outside user traffic into the 1990's. The high- and low-traffic estimates for LEO spacecraft through 1990 are presented in Tables 5.1-1 and 5.1-2. Listed in these tables are a mission name, sponsor, expected service life in years, launch schedule broken down by year, the total number of launches expected (through 1997), and the number of spare satellites being considered for the program. A table of acronyms for the mission names is presented in the Appendix. Totals are presented for each subgroup of missions.

Candidate deployable spacecraft in the latest Shuttle manifest are presented in Table 5.1-3. The manifest runs through 1987. Two additional candidates, the Upper Atmospheric Research Satellite (UARS) and LANDSAT, do not appear in this manifest.

TABLE 5.1-1. HIGH MODEL FOR OUTSIDE USER TRAFFIC INTO LOW EARTH ORBIT

MISSION	SPONSOR	SERVICE LIFE	LAUNCH SCHEDULE								TOTAL THRU 1997	GROUND SPARE
			83	84	85	86	87	88	89	90		
<u>U.S. LOW EARTH ORBIT OBSERVATIONS</u>												
TIROS N SERV NOAA -D (NOAA-8R)	NOAA	2	0	1	0	0	0	0	0	0	1	1
ATN-ADV TIROS N NOAA-E,-F,-G (NOAA-8,9,10)	NOAA	2	1	0	1	1	0	0	0	0	3	0
ADV TIROS-N NOAA-H THRU -K NOAA-11 THRU -14	NOAA	2	0	0	0	0	1	0	1	1	4	0
NOAA F/O	NOAA	2	0	0	0	0	0	0	0	0	3	0
OPERATIONAL EARTH RESOURCES	U.S. GOV'T	0	0	0	0	0	0	0	0	1	7	0
OPERATIONAL EARTH RESOURCES	INDUSTRIAL GROUP	0	0	0	0	0	0	0	0	0	3	0
MAPSAT (OPERATIONAL LAND OBS SYS)	US GOV'T	10	0	0	0	0	0	0	1	0	3	0
AEROS (ADV EARTH RESOURCE OPS SAT)	ASTEC (AMER, SCI, & TECH, CO)	5	0	1	1	1	1	0	0	0	4	0
AEROS F/O	ASTEC	5	0	0	0	0	0	0	0	1	4	0
TOTAL			1	2	2	2	2	0	2	3	32	
<u>FOREIGN LOW EARTH ORBIT OBSERVATIONS</u>												
ERS-1 FORM, MERES (WAS ERSS & LOS PG'M)	JAPAN NASDA	2	0	0	0	0	1	0	1	0	2	
ERS F/O	NASDA	2	0	0	0	0	0	0	0	0	4	
GS-1 (GEOLOGICAL SAT)	NASDA	0	0	0	1	0	0	0	0	0	1	
MOS-1,-2,-3 (MARINE OBSERVA- TION SAT)	NASDA STA	0	0	0	0	1	0	0	1	0	3	
LOS-1 (LAND OBS SAT)	NASDA STA	0	0	0	0	0	0	0	0	1	2	

TABLE 5.1-1. (Continued)

MISSION	SPONSOR	SERVICE LIFE	LAUNCH SCHEDULE							TOTAL THRU 1997	GROUND SPARE	
			83	84	85	86	87	88	89			90
<u>FOREIGN LOW EARTH ORBIT OBSERVATIONS (Cont'd)</u>												
OPERATIONAL LEO SAT	JAPANESE GOV'T INDUSTRY	0	0	0	0	0	0	0	0	0	2	
OPERATIONAL LEO SAT, F/O	NASDA STA MITI	0	0	0	0	0	0	0	0	0	2	
RADARSAT OPERATIONAL	CANADA	5	0	0	0	0	0	0	0	1	3	
ERS-1 (ESA RESOURCE SAT,1)	ESA	0	0	0	0	0	1	0	0	0	1	
AERS (ADVANCED ERS) ERS)	ESA	0	0	0	0	0	0	0	1	0	3	
AERS F/O	ESA	0	0	0	0	0	0	0	0	0	2	
SPOT -1,-2,-3 -4	FRANCE SWEDEN	4	0	1	0	1	0	1	0	1	4	0
SPOT F/O	FRANCE	4	0	0	0	0	0	0	0	0	2	0
OPERATIONAL LEO	EUROPEAN GOV'T INDUSTRY	0	0	0	0	0	0	0	0	0	5	0
BERS (BRAZIL EARTH RESOURCES SAT)	BRAZIL	2	0	0	0	1	0	1	0	0	2	0
BERS F/O	BRAZIL	2	0	0	0	0	0	0	0	1	3	0
BMETEO SAT (BRAZIL'S METEO- ROLOGICAL SAT)	BRAZIL	2	0	0	1	0	1	0	0	0	2	0
BMETEO F/O	BRAZIL	2	0	0	0	0	0	0	1	0	4	0
CHINASAT -10 EARTH OBS	CHINA (P.R.C.)	2	0	1	0	0	0	0	0	0	2	0
CHINASAT -12 EARTH RESOURCES	CHINA (P.R.C.)	2	0	0	1	0	1	0	0	0	2	0

TABLE 5.1-1. (Continued)

MISSION	SPONSOR	SERVICE LIFE	LAUNCH SCHEDULE								TOTAL THRU 1997	GROUND SPARE
			83	84	85	86	87	88	89	90		
<u>FOREIGN LOW EARTH ORBIT OBSERVATIONS (Cont'd)</u>												
LEO OBS SATELLITES	CHINA (P.R.C.)	2	0	0	0	0	0	0	1	0	4	0
CHINA METEO SATELLITE	CHINA (P.R.C.)	2	0	0	0	0	1	0	0	1	4	0
MILITARY RECON	CHINA (P.R.C.)	2	0	1	0	0	0	0	0	0	1	0
MILITARY RECON F/O (IMPROVED)	CHINA (P.R.C.)	2	0	0	0	1	0	1	0	1	3	0
IRS-1 EXP. EARTH SENS'G SAT (IRS-1)	ISRO INDIA	2	0	1	0	0	0	0	0	0	1	0
IRS -2	ISRO INDIA	2	0	0	0	0	1	0	0	0	1	0
PROTO IRS	ISRO INDIA	2	0	0	1	0	0	0	0	0	1	0
ADVANCED IRS	ISRO INDIA	2	0	0	0	0	0	1	0	0	2	0
IRS F/O	ISRO INDIA	2	0	0	0	0	0	0	0	0	2	0
SAMRO	FRANCE	4	0	0	0	0	1	1	0	0	5	0
TERS (TROPICAL EARTH RESOURCES SAT)	INDONESIA	0	0	0	0	0	0	0	0	0	2	0
TOTAL			0	4	4	4	7	5	5	6	77	
<u>NAVIGATION AIDS</u>												
TRANSIT 49-50 NOVA 2-3	U.S. NAVY	4	1	0	0	0	0	0	0	0	2	0
TRANSIT 21 & 26	U.S. NAVY	0	1	0	0	0	1	0	0	0	2	0
TRANSIT 22-25	U.S. NAVY	0	0	2	0	2	0	0	0	0	4	0
TOTAL			2	2	0	2	1	0	0	0	8	

TABLE 5.1-2. LOW MODEL FOR OUTSIDE USER TRAFFIC INTO LOW EARTH ORBIT

MISSION	SPONSOR	SERV. LIFE	LAUNCH SCHEDULE								TOTAL THRU 1997	GROUND SPARE
			83	84	85	86	87	88	89	90		
<u>U.S. LOW EARTH ORBIT OBSERVATIONS</u>												
TIROS N SERV NOAA -D (NOAA-8R)	NOAA	2	0	0	0	0	0	0	0	0	0	1
ATN-ADV TIROS N NOAA-E,-F,-G (NOAA-9,10,11)	NOAA	2	1	0	1	0	1	0	0	0	3	0
ADV TIROS-N NOAA-H THRU -K NOAA-12 THRU -15	NOAA	2	0	0	0	0	0	0	1	0	4	0
NOAA F/O	NOAA	2	0	0	0	0	0	0	0	0	1	0
OPERATIONAL EARTH RESOURCES	U.S. GOV'T	0	0	0	0	0	0	0	0	0	4	0
OPERATIONAL EARTH RESOURCES	ASTEC	5	0	1	0	1	0	1	0	1	4	0
TOTAL			1	1	1	1	1	1	1	1	16	
<u>FOREIGN LOW EARTH ORBIT OBSERVATIONS</u>												
ERS-1 FORM, MERES (WAS ERSS & LOS PG'M)	JAPAN'S MITI NASDA	2	0	0	0	0	0	0	1	0	1	0
GS-1 (GEOLOGICAL SAT)	NASDA	0	0	0	0	1	0	0	0	0	1	0
MOS-1 (MARINE OBSERVA- TION SAT)	NASDA STA	0	0	0	0	0	0	1	0	0	1	1
LOS-1 (LAND OBS SAT)	NASDA STA	0	0	0	0	0	0	0	0	0	1	0
OPERATIONAL LEO SAT, F/O	MASDA STA MITI	0	0	0	0	0	0	0	0	0	2	0
RADARSAT (OPERATIONAL)	CANADA	5	0	0	0	0	0	0	0	0	1	0
ERS-1 (ESA RESOURCE SAT.1)	ESA	0	0	0	0	0	0	0	1	0	1	0

TABLE 5.1-2. (Continued)

MISSION	SPONSOR	SERV. LIFE	LAUNCH SCHEDULE								TOTAL THRU 1997	GROUND SPARE
			83	84	85	86	87	88	89	90		
<u>FOREIGN LOW EARTH ORBIT OBSERVATIONS (Cont'd)</u>												
SPOT -1,-2,-3 -4	FRANCE SWEDEN	2	0	1	0	0	0	1	0	0	4	0
OPERATIONAL LEO	EUROPEAN GOV'T INDUSTRY	0	0	0	0	0	0	0	0	0	2	0
BMETEO SAT (BRAZIL'S METEOR- LOGICAL SAT)	BRAZIL	2	0	0	0	1	0	0	1	0	2	0
CHINASAT -10 EARTH OBS	CHINA (P.R.C.)	2	1	0	0	0	0	0	0	0	1	0
LEO OBS SATELLITES	CHINA (P.R.C.)	2	0	0	0	1	0	0	1	0	5	0
CHINA MATEO SATELLITE	CHINA (P.R.C.)	2	0	0	1	0	0	1	0	0	2	0
MILITARY RECON	CHINA (P.R.C.)	2	0	0	1	0	0	1	0	0	2	0
IRS-1 INDIA REMOTE SENSING	ISRO INDIA	2	0	1	0	0	0	0	0	0	1	0
IRS -2	ISRO INDIA	2	0	0	0	0	1	1	0	0	1	0
PROTO IRS	ISRO INDIA	2	0	0	1	0	0	0	1	0	2	0
SAMRO	FRANCE	4	0	0	0	0	0	1	1	0	4	0
TOTAL			1	2	3	3	0	6	6	0	34	
<u>NAVIGATION AIDS</u>												
TRANSIT 49-50 NOVA 2-3	U.S. NAVY	4	1	0	0	0	0	0	0	0	2	0
TRANSIT 21 & 26	U.S. NAVY	0	1	0	0	0	1	0	0	0	2	0
TRANSIT 22-25	U.S. NAVY	0	0	2	0	2	0	0	0	0	4	0
TOTAL			2	2	0	2	1	0	0	0	8	

TABLE 5.1-3. DEPLOYABLE LOW EARTH ORBIT SATELLITES APPEARING
IN THE LATEST SHUTTLE MANIFEST

Payload Name	Scheduled Flight	Expected Launch Date
LDEF-1	13	4/13/83
ERBS	17	7/28/84
EOS-1	24	1/30/85
EOS-2	31	9/ 1/85
CRRES	33	10/24/85
Eureca	55	4/11/87
LDEF-2	57	5/19/87
ROSAT	60	7/24/87
EUVE	63	9/20/87

Acronyms:

Long Duration Exposure Facility (LDEF)
 Earth Radiation Budget Satellite (ERBS)
 Electrophoresis Operations in Space (EOS)
 Combined Release and Radiation Effects Satellite (CRRES)
 Roentgen Satellite (U.S./German X-ray Explorer) (ROSAT)
 Extreme Ultraviolet Explorer (EUVE)

Candidate DoD spacecraft are not provided on publically issued manifests, but easily exceed the list of NASA candidates. There are 15 DoD-dedicated flights in the current Shuttle manifest, as shown in Table 5.1-4, and DoD payloads appear in 13 other flights as sharees with non-DoD payloads, as shown in Table 5.1-5.

TABLE 5.1-4. DoD-DEDICATED SHUTTLE FLIGHTS APPEARING
IN THE LATEST SHUTTLE MANIFEST

Flight Number	Expected Launch Date
10	11/ 3/83
22	12/ 4/84
23	1/ 5/85
30	8/ 3/85
1V	10/15/85
37	2/15/86
2V	3/ 1/86
42	7/10/86
44	8/21/86
48	11/20/86
4V	1/ 2/87
53	3/ 4/87
5V	3/31/87
62	8/22/87
7V	9/30/87

TABLE 5.1-5. SHUTTLE FLIGHTS CONTAINING BOTH
DoD AND NON-DoD PAYLOADS

Flight Number	Expected Launch Date
34	11/22/85
36	2/ 8/86
41	7/ 2/86
43	8/12/86
45	9/23/86
46	10/ 4/86
47	11/ 7/86
50	1/ 9/87
51	1/21/87
55	4/11/87
57	5/19/87
59	6/27/87
63	9/20/87

The program most likely to be an avenue for sharing on DoD payloads is the USAF Space Test Program (STP) which is managed through USAF/Space Division. The STP provides the service of matching DoD sponsored experiments with available carriers, which might be either free-flyers or attached Shuttle payloads. DMSP and DISCUS have piggy-backed experiments through this program. In joint NASA/DoD ventures of this sort in the past, the sponsoring DoD organization has usually been one of the DoD laboratories. For an IR debris detector, the Geophysics Laboratory would be most likely to show interest, while for radar systems Electronics Systems Division (ESD) or Rome Air Development Center (RADC) would be candidates. The regulation controlling involvement in STP is AF Regulation 80-2.

DoD ELV free-flyers going into LEO through FY 85 are pushing their operational limits and would probably not be good piggy-back candidates. Spacecraft launched in FY 86 and beyond have not been studied by the STP office as yet, but such studies are expected to begin by the end of FY 1983. It does not appear likely that a DDM piggy-backing on a DoD free-flyer could be in orbit sooner than late 1988.

Opportunities associated with Shuttle payloads seem to be disappearing. Schedule slips and elevating project costs have created an atmosphere in which program managers are not receptive to the imposition of additional instrumentation which potentially jeopardizes modified schedules and spacecraft reliability. The use of DoD carriers would provide a natural means for obtaining NASA/DoD cooperation on understanding the debris problem.

5.2 WORKING FROM THE SHUTTLE IN A NON-DEPLOY MODE

For some applications, riding on the Shuttle as an attached or tethered payload or as a free-flyer to be returned with the Shuttle could offer advantages in a testing and

development program as well as in a monitoring role. Data on the IRAS instrumentation suggests that a cryogenically cooled IR telescope of modest size (15 in.) riding at 300 km could penetrate well into the high debris density region around 850 km at debris sizes of 1 cm and larger. Hence, the instrument could serve a monitoring function if used on occasional flights if the detection rates were sufficient to yield data over the necessarily short Shuttle mission duration.

There appears to be many possibilities for sharing in this role. There is an extensive list of attached multiple-experiment payloads being sponsored by the Office of Space Sciences (OSS), including the SPARTAN payload from the suborbital program, the Office of Space Sciences and Applications (OSTA), and the Office of Aeronautic and Space Technology (OAST). Payloads which appear in the latest manifest are listed in Table 5.2-1. Since these payloads will support a variety of experiments, sharing on some payloads will be easier than on others.

Increased interest is being shown by NASA in making use of excess space on the Shuttle by establishing a pool of non-complex experiments which can be combined onto a single pallet and flown on an as-available basis as attached payloads. A program titled Capabilities for Opportunity Payloads/Experiments (COPE, to be renamed HITCHIKER), currently managed out of MSFC, is going to be presented to NASA Headquarters in the near future. The current plan is to have the first HITCHIKER payload on-board STS-14. A list of opportunity payloads is provided in Table 5.2-2.

Finally, there are a number of non-NASA attached payloads which could be shared for a DDM. These are listed in Table 5.2-3. The SPACELAB payloads are not included in this list, as these payloads are discussed in the next section.

TABLE 5.2-1. NASA-SPONSORED ATTACHED PAYLOADS
SCHEDULED FOR SHUTTLE FLIGHTS

Payload Name	Flight Number	Expected Launch Date
OSTA-2	7	5/83
OAST-1	14	5/ 8/84
SPARTAN-1	16	7/ 1/84
OSTA-3	17	7/28/84
OSTA-4	20	10/11/84
OAST-2	27	5/14/85
SPARTAN-2	33	10/24/85
OSTA-5	36	2/ 8/86
OSS-5	38	3/25/86
OSS-6	47	11/ 7/86
OSTA-6	49	12/ 4/86
OSTA-8	55	4/11/87
SPARTAN-3	55	4/11/87
OSTA-7	6V	6/15/87
OSS-7	59	6/27/87
OAST-3	63	9/20/87

TABLE 5.2-2 SHUTTLE FLIGHTS CONTAINING AVAILABILITY
FOR OPPORTUNITY PAYLOADS

Flight Number	Expected Launch Date
14	5/ 8/84
17	7/28/84
20	10/11/84
24	1/30/85
29	7/ 9/85
34	11/22/85
3V	8/ 1/86
6V	6/15/87
60	7/24/87

TABLE 5.2-3 SHUTTLE FLIGHTS CONTAINING NON-NASA SPONSORED
ATTACHED PAYLOADS

Payload Name	Flight Number	Expected Launch Date
LFC-1	11	1/29/84
MEA-1	12	3/18/84
MPS-1	33	10/24/85
MPS-2	52	2/10/87

Acronyms:

Large Format Camera (LFC)
Materials Experiment Assembly (MEA)
Materials Processing in Space (MPS)

5.3 USING DATA ACQUIRED IN OTHER CONTEXTS

The possibility for debris detection introduced by the launching of the IRAS satellite underscores the possibility for obtaining debris data at virtually no marginal cost to NASA. In fact, there may be data that has been thrown away in the past-- although it applies to GEO rather than LEO, it may be that data returned by the GOES satellite has had debris data impacted in it.

For the acquisition of remote sensing data, there are two free-flyers after IRAS which might return useful data - the Space Telescope, to be launched on STS-26 in 1985, and EUVE, to be launched on STS-63 in 1987. In both cases it would be sunlight scattered off the debris which would be detected. The Spacelab flights, having experiments in astronomy and solar physics as well as other fields, will have requirements compatible with collecting debris data; the numerous flights, as listed in Table 5.3-1, might form the foundation for a debris monitoring program.

TABLE 5.3-1 SPACELAB FLIGHTS SCHEDULED ON
THE CURRENT SHUTTLE MANIFEST

Spacelab Designator	Flight Number	Expected Launch Date
1	9	9/30/83
2	25	2/26/85
3	19	9/15/84
D-1	28	6/11/85
4	35	12/17/85
D-4	54	3/21/87
6	56	5/ 1/87
8	61	8/ 4/87

Any spacecraft which is introduced into the environment and then returned to the Shuttle bay for return to Earth represents a potential "impact counter". Such spacecraft include long-term deployable/retrievable carriers such as LDEF and Eureca, and short-term non-deployables which are left outside the Shuttle during Shuttle mission duration. Inexpensive procedures such as special surface preparation might be used on these carriers to enhance the quality of the data with minimal marginal cost.

TABLE 5.3-2 DEPLOYMENT/RETRIEVAL OF RETRIEVABLE CARRIERS

Payload Name	Deploy/Retrieve	Flight Number	Expected Launch Date
LDEF-1	D	13	4/13/83
LDEF-1	R	26	4/18/85
LANDSAT	R	3V	8/1/86
EURECA	D	55	4/11/87
LDEF-2	D	57	5/19/87
EURECA	R	63	9/29/87

6.0 CONCLUSIONS

In the area of population definition and population evolution, a significant discrepancy exists between BCL and JSC modeling results. This is due in part to a difference in the definition of the zero-time population, but may also involve the difference in modeling techniques.

A high priority should be placed on resolving this discrepancy. Part of the effort should be directed towards establishing one or more zero-time reference populations to serve as standard initial conditions for evolutionary modeling. Once the zero-time standards are established, bench mark evolutionary calculations should be performed to verify the validity of the various modeling techniques.

Once satisfactory debris state projections have become available, the issue of spacecraft vulnerability to debris impact can be addressed. For those space programs having vehicles requiring protection from objects larger than milligram in size, so that simple spacecraft shielding would require an unacceptable weight penalty, an adequate vulnerability analysis would be required to consider programmatic and operational alternatives as well as structural and design layout alternatives. Vulnerability analysis concepts for these latter alternatives might be carried over from aircraft vulnerability studies.

A number of important conclusions were reached in the area of remote sensing detectors. For ground-based systems, there is no radar system capable of detecting smaller than 2 cm objects at lowest orbital altitudes; the PARCS radar has the best performance for detecting small objects. Achieving significant improvements in detection ranges on small particles with ground-based radar does not, in practice, appear feasible. The GEODSS system, which is optical, has the capability to detect millimeter sized debris in LEO for stationary targets, but its capability

is

C-2

for detecting moving targets cannot be determined using unclassified information.

For current space-based detector systems, there is no radar system which is suitable. However there is a space-qualified power amplifier which has been flown on GEOS and SEASAT and which would be suitable for building a near-term space-qualified radar system in the 13-15 Ghz frequency range. Such near-term systems would be of value only if sufficient detection ranges could be obtained. Far-term systems employed in non-conventional detection modes--such as using sequential detection or staring modes--could be used to improve effective sensitivity and therefore increased detection range for a given size of debris.

Future radar debris detectors, being active systems, will be inherently more complex, more expensive, and less reliable than passive systems, but might also provide more useful data on the debris population properties. In an experimental system, a radar detector would not be able to compete on a cost basis with a passive system, but if an ongoing monitoring program was established the radar, by providing range, size, and velocity information directly in the data, would compete more favorably with passive systems, which can provide this data only on a statistical basis.

Some re-evaluation of the specifications of an orbiting radar for debris detection appears to be necessary. In the radar proposed by GE, the detection ranges were such that extremely low detection rates ($<1 \text{ yr}^{-1}$) would be expected. The simultaneous requirements to track at the expected rates for debris detection and to cover a large area result in short integration times, leading to the small detection ranges and a complex phased array radar. Much simpler systems with greater detection ranges could be employed if the primary design requirement was to detect and it would appear that a detection-driven design should be considered.

Space-based electro-optical detectors are in use on the IRAS, a multiband IR telescope. The sensitivity parameters of this instrument would indicate that it is capable of detecting millimeter sized debris to a distance of 70 km, if the debris is moving through the field of view "sufficiently slowly". However, as was the case with the GEODSS instruments, the effective sensitivity for rapidly moving targets will be less. The information needed to determine what constitutes a rapidly moving target and what this sensitivity becomes for these targets is not classified and steps should be taken to integrate this information in an assessment of the IRAS potential for debris detection. This assessment will be required to interpret the IRAS data currently being acquired in any case, so such a study would serve a two-fold purpose.

The IR technology capability exhibited by IRAS would make future IR debris detectors an attractive possibility. However, at the wavelengths being scanned by IRAS, the need for cryogenics would increase the detector costs. The possibility of using debris detectors in a non-deployed mode on the Shuttle may make the cryogenically cooled detectors a viable option for an ongoing monitoring role, even though the cost associated with such an option is generally formidable for space-based detectors.

A passive optical system, which would not require cryogenic cooling, may be the least expensive option to pursue. However, to understand the performance of such a system, the effect of target motion and target scintillation on the effective sensitivity needs to be evaluated.

It has become apparent that in order to intelligently select an orbital sensor or sensors for debris monitoring purposes, the relationship between the data collecting capabilities of the sensors, such as collection areas, sampling rates, detection ranges, position and velocity accuracies, etc., and the data input requirements for the modeling activity, such as debris particle size, velocity, and spatial distribution, must be known

or established. This allows a "figure of merit" to be assigned to a particular sensor with respect to its capabilities for providing the data required to achieve a given monitoring objective. Subsequent evaluation of the physical characteristics and resource requirements (i.e. power, weight, reliability, cost, etc.) of various sensor configurations relative to this merit in the debris monitoring task should allow selection of an optimum sensor configuration.

It is recommended that such an assessment be conducted and that further comparative evaluations of the radar, optical, and IR sensors be performed. A detailed comparison is needed for radar and electro-optical detectors for similar scan volumes and for different orientations of the scan volume relative to the detector velocity vector. Within the radar option, trade-offs in a number of different design options should be made.

Over the next 15 years there will be many potential carriers for LEO debris detection devices. These will include free-flyers, the Shuttle, and non-deployed experiments aboard the Shuttle. The availability of the Shuttle, payloads which remain on the Shuttle, and carriers which are retrieved by the Shuttle opens up the option for utilizing debris monitoring modules which would record data locally and not need a telemetry interface.

There will also be a number of opportunities to obtain debris data at minimal marginal cost from experiments or programs being conducted for other purposes. For detection of large particles, data acquired from orbiting astronomical instruments such as IRAS, Space Telescope, EUVE, and some of the Spacelab modules might have impacted debris data; if such a possibility exists, input to the program office involved might be needed to prevent debris data from being discarded during on-board data processing. Retrievable carriers such as LDEF and Eureka should be used routinely as microparticle impact counters by conducting inspection of the spacecraft surface after retrieval. Special surface preparation might be used at minimal marginal cost to enhance the quality of data obtained in this manner.

7.0 REFERENCES

Alexander, W. M. and Berg, O. E., ed. 1961. "Proceedings of the Fifth Symposium on Hypervelocity Impact".

Aumann, H. H. and Walker, R. G. 1977. "Infrared Astronomical Satellite", Optical Engineering, 16, 6, November-December.

Berg, O. E. and Meredith, L. H. 1956. "Meteorite Impacts to Altitude of 103 km", Journal of Geophysical Research, 61, 751.

Bess, T. D. 1975. "Mass Distribution of Orbiting Man-Made Space Debris", NASA Technical Note TND-8108.

Chobotov, V.A. 1981. "Collision Hazard in Space", The Aerospace Corporation Report TR-0081(6790)-1, February.

Cour-Palais, B.G. 1969. "Meteoroid Environment Model-1969 (Near Earth to Lunar Surface), NASA SP-8013.

Friichtericht, J. F. 1961. "Study of Crater Physics", STL Report No. 8980-0003-RU-000, Final Report, NASA Contract NAS5-763.

Humes, D. H. 1981. "Meteoroid Bumper Experiment on Explorer 46", NASA TN-1879.

Humes, D. H., Alvarez, J. M., O'Neal, R. L., and Kinard, W. H. 1974. "The Interplanetary and Near Jupiter Meteoroid Environment", Journal of Geophysical Research, 79, #25, September 1.

Jurkevich, I. 1971. "Earth Orbiting Sisyphus System Study", General Electric Company, NASA CR-112024, October.

Kessler, D. J. and Cour-Palais, B. G. 1978. "Collision Frequency of Artificial Satellites: The Creation of a Debris Belt", Journal of Geophysical Research, 83, June 1, 2637-2646.

Kessler, D. J. 1981. "Sources of Orbital Debris and the Projected Environment for Future Spacecraft", Journal of Spacecraft and Rockets, 18, 4, 357-360.

Kessler, D. J. 1982. "Proposed Preliminary Design Criteria-- Model Environment for the 1990's", presented at the Johnson Space Center Orbital Debris Workshop, July 27.

~~PRECEDING PAGE BLANK NOT FILMED~~

**ORIGINAL PAGE IS
OF POOR QUALITY**

7-2

Kessler, D. J. 1982a. "Impacts on Explorer 46 from an Earth Orbiting Population", presented at the Johnson Space Center Orbital Debris Workshop, July 27.

Kessler, D. J. 1982b. "NORAD's PARC's Small Satellite Tests (1976 and 1978)", presented at the Johnson Space Center Orbital Debris Workshop, July 27.

LeGalley, D. P. and Rosen, A., ed. 1964. "Space Physics", John Wiley & Sons, Inc., New York, NY.

Reynolds, R. C., Fischer, N. H., Edgecombe, D. S. 1982. "A Model for the Evolution of the On-Orbit Man-Made Debris Environment", IAA-82-155, presented at the 1982 IAF Paris Meeting, September, 29.

Roberts, B. 1982. "Particles Smaller than 1 mm", Presented at the Johnson Space Center Orbital Debris Workshop, July 27.

Smith, B. A. 1979. "Ground-Based Electro-Optical Deep Space Surveillance System", Aviation Week and Space Technology, August 27.

Soberman, R. K. 1974. "Optical Measurement of Interplanetary Particulates from Pioneer 10", Journal of Geophysical Research, 79, #25, September 1.

"The 1969 Aerospace Yearbook", Books, Inc., Washington, D.C.

PRECEDING PAGE BLANK NOT FILMED

**ORIGINAL PAGE IS
OF POOR QUALITY**

APPENDIX A

OUTSIDE USERS PAYLOAD MODEL ACRONYM LIST

(for Tables 5.1-1 and 5.2-2)

- ABCS** - Australian Broadcast Communication Satellite
ACTS - Advanced Communications Technology Satellite (Japan - NASDA)
AMES - Aeronautical Maritime Engineering Satellite (Japan - NASDA)
AOTS - Advanced Orbital Test Satellite (ESA)
ASCO - Arab Satellite Communications Organization
ASETA - (Sp./Ec.) Asociacion de Empresas Estatales de Telecommunications del Acuerdo Sub Regional Andino, (The Andean Satellite Telecommunications Group)
ASTRO - ASTROphysical Satellite (Japan - TU-ISAS)
CNES - (Fr.) Centre National d'Etudes Spactiales (National Center for Space Studies)
COMSS - Coastal Ocean Monitoring Satellite System (ESA)
COMSAT - Communications SATellite Corporation (U.S.)
CXGT - Cooperative X-Ray Telescope (NASDA/NASA)
DOMSAT - DOMestic SATellite (Australia - former name for ABCS)
DUETTO - A standard design spacecraft designed for a dual launch on Ariane with SYLDA. The spacecraft can be equipped with various mission payloads ranging from 88 to 330 pounds.
EBS - Experimental Broadcast Satellite (Japan - NASDA)
ELV - Expendable Launch Vehicle
ERS - Earth Resources Satellite (Japan - NASDA)
EUMETSAT - European METEorological SATellite Organization formed to operate Meteosat and Opmet for eleven ESA member countries.
EUTELSAT - European TELEcommunication SATellite organization formed in 1979 with 15 member countries to manage Europe's communication satellite systems, such as: OTS, ECS, and follow-ons.
ESA - European Space Agency

- GEO - Geostationary Equatorial Orbit
- GIOTTO - Halley's Comet Mission - ESA is calling Giotto after the Florentine painter Giotto di Bondone who included the appearance of Halley's Comet in the year 1301 in the background of his "Adoration of the Magi".
- GLODOM - GLOBAL DOMestic Satellite (UN-ITU)
- GS - Geodetic Satellite (Japan - NASDA)
- HESP - High Energy Solar Physics Satellite (Japan - NASDA)
- HIPPARCOS - High Precision PARallax COLlecting System (ESA)
- INMARSAT - INTERNational MARitime SATellite organization was activated in 1979 to manage and promote implementation of maritime satellite communications systems.
- INTELSAT - INTERNational TELEcommunication SATellite (The name can represent the management organization or the satellites which it procures and operates.)
- IOC - Initial Operational Capability
- IRTS - InfraRed Telescope Satellite (Japan - ISAS)
- ISAS - Institute of Space and Aeronautical Sciences (Tokyo University, Japan)
- ISRO - Indian Space Research Organization
- L-SAT - Large SATellite (ESA's direct broadcast Television Satellite)
- LASS - Land Application's Satellite System (ESA)
- LEO - Low Earth Orbit
- LOS - Land Observation Satellite (Japan - NASDA)
- MBB - (Gr.) Messerschmitt-Bolkow-Blöhm GmbH

- MINOS - (Fr.) Modules Industriels Orbitaux Specialises (Specialized
Orbital Industrial Modules)
- MITI - Ministry of International Trade and Industry (Japan)
- MOS - Maritime Observation Satellite (Japan - NASDA)
- NASA - National Aeronautics and Space Administration (U.S.)
- NASDA - National Space Development Agency (Japan)
- NATO - North Atlantic Treaty Organization
- NIG - Nortic Industrial Group
- NOAA - National Oceanographic and Atmospheric Administration (U.S.)
- OPEN-J - Origin of Plasma in Earth's Neighborhood - Japan (NASDA)
- PATU - Pan-African Telecommunication Union PANAFTEL
- SATCOL - SATellite COLumbia
- SPAS - Shuttle Pallet Satellite
- SPOT - (Fr.) Systeme Probatoire d'Observation de la Terre (Probationary
Earth Observation System)
- STS - Space Transportation System (U.S.) (Space Shuttle System)
- SYLDA - (Fr.) SYsteme de Lancement Double "Ariane" (System for a double
launch on Ariane)
- TDF - (Fr.) Telediffusion de France (Television Broadcasting of France)
- TU-ISAS - Tokyo University's Institute of Space and Aeronautical Sciences
- UN-ITU - United Nations International Telecommunications Union